Atmospheric
Chemistry
and Physics
Discussions

Vertical variability of the properties of highly aged biomass burning aerosol transported over the southeast Atlantic during CLARIFY-2017

Huihui Wu[1], Jonathan W Taylor[1], Kate Szpek[2], Justin Langridge[2], Paul I Williams[1, 3], Michael Flynn[1], James D Allan[1, 3],Steven J Abel[2], Joseph Pitt[1, 5], Michael I Cotterell[2, 4, 6], Cathryn Fox[2], Nicholas W Davies[2, 4], Jim Haywood[2,4] and Hugh Coe[1]

[1]Department of Earth and Environmental Sciences, University of Manchester, Manchester, UK
[2]Met Office, Fitzroy Road, Exeter, EX1 3PB, UK
[3]National Centre for Atmospheric Science, University of Manchester, Manchester, UK
[4]College of Mathematics, Engineering and Physical Science, University of Exeter, UK.
[5]Now at: School of Marine and Atmospheric Science, Stony Brook University, Stony Brook, US
[6]Now at: School of Chemistry, University of Bristol, Bristol, UK, BS8 1TS

Correspondence to: Hugh Coe (hugh.coe@manchester.ac.uk)

Abstract. Seasonal biomass burning (BB) from June to October in central and southern Africa leads to absorbing aerosols being transported over the south Atlantic Ocean every year, and contributes significantly to the regional climate forcing. The vertical distribution of submicron aerosols and their properties were characterized over the remote southeast Atlantic for the first time, using airborne in-situ measurements made during the CLoud-Aerosol-Radiation Interactions and Forcing for Year 2017 (CLARIFY-2017) campaign. BB aerosols were intensively observed in the region surrounding Ascension Island, in the marine boundary layer (MBL) and free troposphere (FT) up to 5 km. We show that the aerosols had undergone a significant aging process during >7 days transit from source, as indicated by highly oxidized organic aerosol and thickly coated black carbon (BC). The highly aged BB aerosols in the CLARIFY region were also especially rich in BC compared with those from other regions.

We also found significant vertical variation in the single scattering albedos (SSA) of these aerosols, as a function of relative chemical composition and size. The lowest SSA was generally in the low FT layer around 2000 m altitude (medians: 0.83 at 405 nm and 0.80 at 658 nm). This finding is important since it means that BB aerosols across the east Atlantic region are more absorbing than is currently represented in climate models. Furthermore, in the FT, we show that SSA increased with altitude and this was associated with an enhanced inorganic nitrate mass fraction and aerosol size. This likely results from increased partitioning to the existing particles at higher altitude with lower temperature and higher relative humidity. After entrainment into the BL, aerosols were generally smaller in size than were observed in the FT, and had a larger fraction of scattering material with resultant higher average dry SSA, mostly due to marine emissions and aerosol removal by drizzle. Our results provide unique observational constraints on aerosol parameterizations used in modelling regional radiation

Atmospheric
Chemistry
and Physics
Discussions

interactions over this important region. We recommend that future work should consider the impact of this vertical variability on climate models.

1 Introduction

35

Open biomass burning (BB) is a major source of global trace gases and carbonaceous aerosol particles in the atmosphere. The smoke aerosol emitted from BB is mainly comprised of strongly absorbing black carbon (BC) and fine organic aerosol (OA), whose proportions vary according to vegetation type, oxygen availability and combustion phase (Andreae and Merlet, 2001; Andreae, 2019). As controls continue to reduce aerosol emissions from fossil fuels and a

40 changing climate potentially leads to more fires, the relative impact of BB on climate forcing is expected to increase (Fuzzi et al., 2015).

Seasonal burning of grasslands and agricultural residue occurs between June and October across the central and southern African Savanna, contributing about one-third of the global BB emissions (van der Werf et al., 2010). Previous space-based observations showed that smoke aerosols produced by this burning are primarily transported westward for

45 thousands of kilometers over the south Atlantic region by free tropospheric (FT) winds (Edwards et al., 2006;Adebiyi et al., 2015). These smoke layers typically over-lie vast stretches of marine stratocumulus clouds (Adebiyi et al., 2015), where they can exert a warming effect by absorbing both downwelling solar radiation and that scattered upwards from the low-lying clouds (Samset et al., 2013). This radiative effect is sensitive to the smoke's single-scattering albedo (SSA), which is a function of aerosol composition and size and evolves with particle age (Abel et al., 2005). Space-based and in-situ field

50 observations also suggested that the smoke layers can be entrained into the marine boundary layer (MBL) during its transport from land over ocean (Painemal et al., 2014; Zuidema et al., 2018; Haslett et al., 2019a). A recent study suggested that the structure of the mesoscale cellular convection could be important for transporting aerosol from the FT down into the MBL (Abel et al., 2019). The entrained aerosols can directly affect cloud microphysics by acting as cloud condensation nuclei (CCN) (Gordon et al., 2018). BC below clouds could also enhance the formation of convection by providing additional

55 heating within the sub-cloud layer (Koch and Del Genio, 2010).

BB emission in Africa has been shown to be relatively stable on multi-annual timescales (Voulgarakis et al., 2015), implying that transport of African BB aerosols (BBA) across the Atlantic region was likely a consistent phenomenon over past decades. Although BB transport regions have lower aerosol concentrations than areas closer to the source, the large spatial coverage means that their contribution to the regional/global-average forcing will be important. Moreover, the

60 Southeast Atlantic has persistent overlying semi-permeant stratocumulus cloud and therefore aerosol cloud interactions in this specific transport region are strong.

Gordon et al. (2018) simulated the effects of smoke aerosols transported from Africa over the southeast Atlantic area near Ascension Island in a regional model, reporting substantial regional direct radiative effects of +11 W/m^2, a semi-direct effect of −30.5 W/m^2 and an indirect effect of −10.1 W/m^2. This implies an overall cooling effect and highlights the

65   important climate effect of transported BBA over the southeast Atlantic region. The extent to which smoke layers over the Atlantic Ocean subside and entrain into the MBL varies between different models (Peers et al., 2016; Das et al., 2017). Some modelled BB smoke layers quickly descend to lower levels just off the western coast of the continent, whereas space-based observations suggest that smoke layers continue their horizontal transport at elevated levels above the MBL for thousands of kilometres (Das et al., 2017). This is crucial because the simulated aerosol effects are dependent on the vertical distribution

70   of aerosol (especially with respect to clouds), and whether the absorbing aerosols is present within, below or above the cloud (Samset et al., 2013). The uncertainty in simulated aerosol vertical distribution would cause a significant diversity in modelled climate forcing over the region (e.g. Zuidema et al., 2016; Haywood et al., 2020, in prep). Furthermore, uncertainty in SSA is also one of the largest sources of uncertainty in estimating the aerosol direct effects (McComiskey et al., 2008). To improve simulations of aerosol radiative effects, it is vital to constrain models using observational studies.

75   Satellite-based observations have been employed in this region, but the ability of remote-sensing methods to infer the presence of BBA in the MBL and quantify its microphysical and optical properties is limited, since observations are often obscured by clouds. Due to the persistent stratocumulus cloud deck over the south Atlantic, there is little MBL data that is not affected by clouds. The altitude of the aerosol layer in the FT as determined by remote-sensing methods has been reported to be over-estimated (e.g. Rajapakshe et al., 2017). Furthermore, satellite retrievals provide column-integrated

80   aerosol properties and fail to provide information on the large vertical variabilities in aerosol properties. In-situ ground-based measurements, such as those taken on Ascension Island in the southeast Atlantic (Zuidema et al., 2018), inherently lack detailed aerosol vertical information. Co-located lidar on Ascension Island is informative but without spatial coverage.

Previous key aircraft measurements focusing on the southern African BB include SAFARI-2000 (the Southern African Regional Science Initiative) campaign in September 2000 (Haywood et al., 2003a, b). Fresh BB smoke in SAFARI-2000

85   was observed on a single flight directly over a terrestrial large fire (on 13 September 2000), aged smoke was observed from flights over the continent or near the Namibian coast and a single profile of BBA was analysed close to Ascension Island. More recently, the NASA ORACLES (ObseRvations of Aerosols above CLouds and their intEractionS) campaigns in September 2016, August to September 2017 and October 2018 extended measurements over the south Atlantic, and frequently sampled westward of the SAFARI region, but still near the coast (Zuidema et al., 2016; Pistone et al., 2019). The

90   AEROCLO-sA (Aerosols Radiation and Clouds in southern Africa) campaign in August to September 2017, also focused on BBA just before crossing the Namibian coast (Formenti et al., 2019). The DACCIWA (Dynamics-Aerosol-Chemistry-Cloud Interactions in West Africa) campaign in June to July 2016, reported aged BBA that were transported from the southern Africa to both the FT and MBL near the southern coastal region of West Africa (Haslett et al., 2019a, b). Although these aircraft measurements covered African BBA with different ages, they did not provide a broad-scale picture of long-range

95   transported BBA over the remote southeast Atlantic. Observations of the vertical distribution of transported BBA over the remote southeast Atlantic are therefore essential to providing better constraints on future climate model studies in this region.

This study uses data from the CLARIFY-2017 (CLoud-Aerosol-Radiation Interactions and Forcing for Year 2017) aircraft campaign which was conducted in August-September 2017, based from Ascension Island in the southeast Atlantic

Ocean. The spatial distribution of MODIS-detected fires for August 2017 is shown in Fig 1, with the average wind fields at
925 hPa and 700 hPa, corresponding to levels in the BL and FT separately. The burning mostly occurred in central and
southern Africa (0 – 20 S) during the campaign period. Large quantities of BBA generally occurs in a deep, turbulent,
surface-heating-driven layer extending to between 3 and 4.5 km (Labonne et al., 2007). The smoke is then be advected
westward over the Atlantic Ocean by the southerly branch of the African easterly jet, as seen in the wind field at around 700
hPa in Fig. 1. The typical atmospheric BL flow, as indicated by the 925 hPa wind field in Fig. 1, follows the climatological
wind pattern of south-easterlies, advecting clean Southern Hemisphere air around the southern Atlantic subtropical
anticyclone. When smoke is transported from Africa over the south Atlantic it encounters the BL that has deepened further
offshore and north of 5°S (Das et al., 2017). Subsiding smoke layers can be entrained into the BL, and mix with clean air
masses that are transported from the southeast to northwest over the Atlantic Ocean. Typically, smoke plumes have
undergone at least 7 days transport since emission before arriving in the BL around Ascension Island (Gordon et al., 2018,
Zuidema et al., 2018). Haywood et al (2020) reported that aerosols sampled in the operating area was of BB origin and also
indicate their age (4 to 10 days). The CLARIFY aircraft campaign provides the opportunity to observe vertical structures of
African BBA transported to the far-field region over the southeast Atlantic.

This paper presents a synthesis of in-situ airborne measurements, including the vertical distribution of submicron
aerosols, their chemical, physical, and optical properties and mixing state using the CLARIFY measurements. We use this
analysis to investigate the main factors influencing BBA properties over the southeast Atlantic after long range transport.

2 Methodology

2.1 Airborne measurements

The measurements described here were made using the UK FAAM (Facility for Airborne Atmospheric Measurements)
BAe-146 Atmospheric Research Aircraft (ARA), which was based out of Ascension Island (7.93 °S, 14.42 °W) in the
southeast Atlantic, as part of the CLARIFY project. 28 scientific flights (designated flight labels from C028 to C055) took
place between 16th August and 7th September 2017. A series of straight and level runs (SLRs) and vertical profiles were
performed during each flight. The flight tracks during the campaign are shown in Fig. 1a. Transit flights, C040-41, which
took place on 26th August are not included since the aircraft was predominately in clean air at high altitude. A summary of
the flights and scientific deployment are provided by Haywood et al. (2020, in prep), while relevant instruments used in this
study are discussed in more detail here.

The Bae-146 facility can provide aircraft position information and conducts routine measurements of standard
atmospheric variables, such as temperature, pressure and winds. Humidity is measured by a CR-2 chilled mirror hygrometer.
The inboard instruments used in this study drew their sample via standard BAe-146 Rosemount inlets, which have sampling
efficiencies close to unity for sub-micron particles (Trembath, 2012; Trembath et al., 2012).

130   The chemical composition of non-refractory submicron aerosols was measured by a compact time-of-flight aerosol mass spectrometer (C-ToF AMS, Aerodyne Research Inc, Billerica, MA, USA) (Drewnick et al., 2005), which provides broad chemical characterization across a complete range of ion mass-charge (*m/z*) ratios. The detailed operation of the AMS, including calibration and correction factors, during aircraft deployment has been described previously (Morgan et al., 2009). The AMS was calibrated using mono-disperse ammonium nitrate and ammonium sulfate particles. A time and composition

135   dependent collection efficiency (CE) was applied to the data based on the algorithm by Middlebrook et al. (2012). The uncertainties of mass concentrations from aircraft AMS are estimated in Bahreini et al. (2009). In this study, the mass concentrations of organic aerosol (OA), sulfate, nitrate and ammonium are determined, and markers ([m/z60] and [m/z44]) are used to provide information on the composition of the OA fraction. Proportional contributions of OA fragment markers, *f*60 and *f*44 were calculated as the ratios of [m/z60] and [m/z44] to the total OA mass concentration respectively. The AMS

140   suffered from a blockage of the inlet during some periods and data collected from six flights (C042-44, C052, C054 and C055) are not available.

The refractory black carbon (rBC; hereafter referred to as BC) was characterized using a single particle soot photometer (SP2, Droplet Measurement Technologies, Boulder, CO, USA). The instrument setup, operation and data interpretation procedures can be found elsewhere (McMeeking et al., 2010;Liu et al., 2010). The SP2 can measure the particles with an

145   optical diameter of 200 – 700 nm, and 70 – 850 nm for BC-containing particles (Liu et al., 2010; Adachi et al., 2016). The SP2 incandescence signal is proportional to the mass of refractory BC present in the particle, regardless of mixing state. The SP2 incandescence signal was calibrated using Aquadag black carbon particle standards (Aqueous Deflocculated Acheson Graphite, manufactured by Acheson Inc., USA), including the correction (0.75) recommended by Laborde et al (2012a). The overall uncertainty of the BC mass concentration calibration is ±20% (Laborde et al., 2012a, b).

150   Aerosol number size distribution was measured via two wing-mounted Passive Cavity Aerosol Spectrometer Probes (PCASP) and an on-board Scanning Mobility Particle Sizer (SMPS). The PCASP uses the intensity of scattered light to measure the size of a particle at 1 Hz, over a nominal diameter range of 0.1–3 μm across 30 channels. Particle size is determined via calibrations using Di-Ethyl-Hexyl-Sebacate (DEHS) and Polystyrene Latex Sphere (PSL) with known size and refractive index (Rosenberg et al., 2012). Mie scattering theory is used to determine the bin sizes by assuming particles are spherical, using a refractive index of 1.54 – 0.027i following Peers et al. (2019). The SMPS sampled from the same inlet

155   as the AMS, measured distributions of particle mobility diameter divided into 26 or 31 logarithmically spaced bins in the range of 20–350 nm. A low-pressure water-based condensation particle counter (WCPC model 3786-LP) was connected to a TSI 3081 differential mobility analyzer (DMA). The SMPS data was inverted based on a ~1 min averaging time only during periods when other continuous data demonstrates that there is limited change in aerosol concentrations and properties (Zhou

160   et al. 2001). The combination of SMPS and PCASP measurements was used to determine size distributions from 20 nm to 3 μm, providing information on the sub-Aitken and accumulation mode aerosol.

The aerosol dry extinction and absorption were measured with the EXSCALABAR instrument (EXtinction, SCattering and Absorption of Light for AirBorne Aerosol Research) which has been developed by the Met Office for use on the ARA

(Davies et al., 2018, 2019; Szpek et al., 2020, in prep). It consists of an array of spectrometers making use of Photo-Acoustic
165   Spectroscopy (PAS) and Cavity Ring-Down Spectroscopy (CRDS) techniques. The dry (RH < 10%) aerosol absorption
coefficient is measured at wavelengths 405, 514 and 658 nm, and dry extinction coefficient is measured at wavelengths 405
and 658 nm. An impactor ensures any aerosol with geometric diameter greater than 1 μm is removed from the sample. The
instrument, including PAS calibration method, is described in detail by Davies et al. (2018) and Cotterell et al. (2019). The
relative contributions of scattering and absorption are given by the Single Scattering Albedo (SSA), which is calculated as:

$$\mathrm{SSA}\ (\lambda) = 1 - \frac{B_{Abs}(\lambda)}{B_{Ext}(\lambda)}$$

170

in which B_{Abs} is the light-absorption coefficient measured by PAS, B_{Ext} is the light-extinction coefficient measured by
CRDS, and λ is the wavelength. The uncertainty in the SSA calculations is related to the corresponding uncertainties in the
extinction and absorption coefficient measurements. The mean SSA uncertainties are determined to be 0.013 and 0.018 at the
wavelengths of 405 and 658 nm respectively when only considering systematic errors (Peers et al., 2019).

175   Carbon monoxide (CO) was measured by a vacuum ultraviolet florescence spectroscopy (AL5002, Aerolaser GmbH,
Germany), with accuracy of ±3% and precision of 1 ppbv (Gerbig et al., 1999). Calibration was performed using in-flight
measurements of a single gas standard and the background signal at zero CO mole fraction. Carbon dioxide (CO_2) was
measured using a Fast Greenhouse Gas Analyzer (FGGA; Los Gatos Research, USA). The instrument setup, operation and
performance on the ARA has been described for several previous aircraft campaigns (O'Shea et al., 2013). The FGGA was
180   calibrated hourly in flight, using a calibration gas standard traceable to the WMO-X2007 scale (Tans et al., 2011) for CO_2.
Liquid water content (LWC) was calculated from 1 Hz measurements by the Cloud Droplet Probe (CDP), with the operation
and calibration of the CDP described in Lance et al. (2010). An LWC value of 0.01 g m^{-3} was used to define a lower
threshold for the presence of cloud.

2.2 Data analysis and classification

185   All measurements reported here were corrected to standard temperature and pressure (STP, 273.15K and 1013.25 hPa)
and in-cloud data was removed. SP2, PAS, CRDS, CO, CO_2 and PCASP data were recorded at 1Hz and were averaged onto
the AMS time base, which recorded data about every 8 – 9 s. SSA was calculated from the averaged PAS and CRDS data.
Particle number concentrations from PCASP were calculated using bins with diameter below 1 μm. SMPS and PACSP size
distributions were averaged over each SLR. Flights with the AMS sampling problem mentioned above (C042-44, C052,
190   C054 and C055), sampling mainly in-cloud (C052-54) or the transits (C040-41), are not considered in the following analysis.
Flights used in this study are listed in Table S1.

Over the southeast Atlantic, there is typically a strong thermodynamic inversion at the top of the BL (e.g. Lock et al.,
2000). The profiles of temperature and specific humidity during the campaign are shown in Fig. S1, the lack of variability
shown by the bars demonstrates the ubiquitous nature of this inversion. Here, we define the BL top to be coincident with the
195   base of the temperature inversion, typically at an altitude around 1400 – 2000 m. The inversion layer sits immediately above

Atmospheric
Chemistry
and Physics
Discussions

the BL and is characterised by a sharp increase in temperature and coincident steep decrease in specific humidity. Above the inversion layer, the air is dry (specific humidity < 0.002 g/kg compared to > 0.01 g/kg in the BL), and is regarded as being in the FT. Using these thermodynamic criteria, we divided the data from each flight into three parts, the BL, the inversion layer and the FT. The inversion layer data are in the transition between the BL below and FT aloft and since their characteristics

200 cannot easily be classified, these data are not used in further analysis. In this study, the air masses perturbed by BB pollutants were identified when BC > 0.1 $\mu g\ m^{-3}$, to prevent the noise at low aerosol concentrations affecting our analysis. Clean BL air masses were selected when CO < 66 ppbv, which corresponds to the lowest 5th percentile of all CO data collected in the BL.

3 Results

205   Fig. 2 shows the average vertical distribution of submicron (PM1, $\mu g\ m^{-3}$) aerosol mass concentration for each flight. PM1 mass concentration was calculated from the AMS non-refractory submicron species and BC mass from the SP2. During the month-long campaign, there was significant variability in measured aerosol loadings at different layers. Three distinct types of aerosol vertical structures were observed, and consequently we divided the campaign into three periods. From 16th to 19th Aug (period 1, C028-C032), aerosols were concentrated in the BL. During period 2 (from 22th to 25th Aug, C033-

210 C039), the FT was polluted, and the BL was mostly clean. During period 3 (from 29th Aug to 5th Sep, C045-C051), the aerosols were observed throughout the BL and FT. The following aerosol characterization (chemical, physical and optical properties) were divided into these periods and different vertical layers (the FT and the BL).

3.1 Aerosol chemical properties

    In this section, we consider the chemical composition of observed PM1 during CLARIFY and percentage contribution

215 of different components to the total mass. We also investigate the vertical variability of the fractional chemical composition. The OA markers and elemental analysis are used to indicate the properties and aging status of observed organics. The enhancement ratios of BC and OA were also calculated to obtain some information on the emission conditions at source and the removal during transport (Yokelson et al., 2013).

3.1.1 Submicron aerosol compositions

220   Average composition ratios of BL and FT aerosols for each period are summarized in Table 1. Detailed vertical distributions of concentrations of different chemical components in each flight are shown in Supplementary Fig. S2. In the BB-polluted FT (periods 2 and 3), the relative chemical composition was similar between flights and periods. The composition fractions (average ± standard deviation) were (61 ± 5) %, (13 ± 3) %, (11 ± 4) %, (8 ± 3) % and (7 ± 2) % for OA, BC, sulfate, nitrate and ammonium respectively. In the BB-polluted BL, chemical composition ratios showed temporal

225 variations, with higher sulfate mass fraction and lower BC and OA mass fractions in period 1 than in period 3. Compared

with the FT BBA, sulfate mass fractions in the BL were about 2–3 times larger, with average values of (30 ± 4) % in period 1 and (21 ± 5) % in period 3. BL ammonium mass fraction was also slightly higher than that in the FT. The linear fitted $NH_{4measured}^+/NH_{4predicted}^+$ ratios (Zhang et al., 2007) in the BL were (0.86 ± 0.01) and (0.99 ± 0.02) for period 1 and 3 respectively, indicating the possible presence of acidic aerosol during the first period. When sulfate is not fully neutralized,

230 nitrate formation is suppressed due to the absence of excess of ammonia, leading to the nitrate mass fraction being negligible. OA and BC accounted for smaller fractions of PM1 in the BL than in the FT.

In the clean BL air masses encountered during period 2, which were representative of a background marine environment, the submicron particle mass (0.23 ± 0.18 µg m^{-3}) was dominated by sulfate (0.14 ± 0.10 µg m^{-3}) with small amounts of OA (0.06 ± 0.07 µg m^{-3}) and negligible other components (see chemical fractions in Table 1). Sulfate mass

235 loadings were significantly enhanced (1.9 ± 0.5 µg m^{-3} in period 1 and 0.7 ± 0.2 µg m^{-3} in period 3) and other aerosol species were present when BB smoke was transported into the BL. Contribution from the marine sulfate background may explain the higher sulfate fraction reported for the BL BBA than the FT. During the DACCIWA project, sampling near the southern coastal region of west African, aircraft observations showed that the sulfate mass fraction was also enhanced in BL BBA compared with the FT BB layer (see Table 1), after long range transport of southern African BB smoke (Haslett et al.,

240 2019b).

Table 1 also compares the chemical composition of BBA measured during CLARIFY and other studies focusing on southern African BB of different ages. The chemical composition of FT non-refractory BBA in CLARIFY is similar to the transported FT BBA in DACCIWA (Haslett et al., 2019b). During SAFARI-2000, off-line methods using filter samples were employed (Formenti et al., 2003). Concentration of water extractable ions (NO_3^-, SO_4^{2-}, NH_4^+) was determined using ion

245 chromatography (IC), and total carbon (TC = organic carbon + elemental carbon) was determined using thermo-optical analysis techniques. The comparison shows composition differences between the fresh and aged BBA (1 – 2 days) in SAFARI-2000 and more aged BBA sampled during the CLARIFY and DACCIWA experiments. The lower OA fraction of more aged BBA is likely due to OA loss after emission as a result of evaporation or oxidation (Yokelson et al., 2009; Cubison et al., 2011), or the formation of the secondary inorganic components (Pratt et al., 2011).

250 We also observed vertical variation in the fractional chemical composition of the BB layers, as shown in Fig. 3. In the BB-polluted FT, the nitrate mass fraction increased with altitude, mean values ranged from 4% to 13% in period 2 and from 6% to 11% in period 3 respectively. The linear fitted C-ToF AMS $NH_{4measured}^+/NH_{4predicted}^+$ ratios of FT aerosols in period 2 and 3 were (1.06 ± 0.01) and (1.05 ± 0.02) respectively, indicating that sulfate in CLARIFY FT aerosols was fully neutralized. Therefore, the concentrations of nitrate, ammonium and sulfate in FT aerosols during periods 2 and 3 were

255 governed by the thermodynamic equilibria between their relative mole fractions rather than acidity. The ammonium mass fraction also slightly increased with altitude, consistent with the higher nitrate mass fraction, while sulfate was relatively constant or slightly decreased. The BC mass fraction generally decreased with altitude in the FT; mean values changed from 14% to 9% in period 2 and from 16% to 12% in period 3. In the BB-polluted BL, there was no significant vertical variability in period 1. In period 3, the sulfate mass fraction increased from 17% at the top of the BL to 23% when close to the surface,

260   while other component mass fractions showed slightly opposite trends (BC and nitrate mass fractions) or were relatively

stable (OA and ammonium mass fractions).

3.1.2 Organic composition and elemental analysis

The OA fragment marker, $f60$, represents the prevalence of anhydrous sugars such as levoglucosan that are known

pyrolysis products of wood burning. Hence, $f60$ is regarded as an indicator of emitted primary aerosol during BB (Schneider

265   et al., 2006;Alfarra et al., 2007). Meanwhile, $f44$ is associated with the CO_2^+ ion and is a marker for oxidized OA (Aiken et

al., 2008). The method used by Cubison et al., (2011) that relies on $f44$ vs. $f60$ to represent the aging of BB OA in the

atmosphere is reproduced in this work. This approach compares the increasing oxidation of the OA (increasing $f44$) with the

oxidative decay of the levoglucosan-like species (decreasing $f60$), allowing a simplified description of BB OA aging to be

compared across different BB studies. Fig. 4 shows the $f44$ vs. $f60$ diagram of the average values in each flight and compares

270   these values with those obtained by previous studies. During CLARIFY, $f60$ was low but generally above the 0.3% that has

been observed as the background level in air masses without BB influence (Cubison et al., 2011) (grey dashed line in Fig. 4).

Average $f60$ were calculated as (0.6 ± 0.3) % and (0.5 ± 0.2) % in the BB-polluted FT and BL respectively. $f60$ is currently

thought to be a robust BB tracer for aging timescales within 1 day from emission (Cubison et al., 2011). However, some

studies assume that the lofting of BB smoke into the FT may lead to the retention of levoglucosan-like species after

275   transportation over extensive temporal and spatial scales (Arangio et al., 2015; Jolleys et al., 2015). Jolleys et al. (2015)

reported a higher $f60$ of (1.2 ± 0.5) % for aged BBA from boreal forest fires than that closer to the source, which had been

transported ~5 days in the FT. It is possible that levoglucosan-like species have a longer lifetime when BBA is transported in

the FT, however, the evidence provided in this paper indicates substantial oxidation has occurred in the far-field after >7

days transport in the FT, and $f60$ would eventually reach low values although it is still above background. Average $f44$ from

280   each flight were mainly in a range of 18 – 23% and 20 – 25% in the BB-polluted FT and BL. As shown in Fig. 4, $f44$ and $f60$

values during CLARIFY lie in the left top of the panel, and $f44$ are at a high level compared with other BB studies in source,

near-source or transport regions (Cubison et al., 2011; Haslett et al., 2019b). These high $f44$ values indicate the large fraction

of oxidized OA (OOA) and/or highly oxidized OA state.

We also calculated the elemental composition ratio of oxygen and carbon (O/C) and organic mass to organic carbon

285   ratio (OM/OC) based on the estimates proposed by Aiken et al. (2008). The uncertainty in the atomic ratio for O/C can be up

to 30% and for OM/OC 6% (Aiken et al., 2008). The O/C ratio is a proxy for oxidation state. O/C ratios were estimated to be

0.77 – 1.0 and 0.82 – 1.03 in the in the BB-polluted FT and BL respectively, which is within the observed values of low-

volatility OOA (LV-OOA) (0.5 – 1.1) (Ng et al., 2011) and dicarboxylic acids (0.4 – 2.0) (Kuwata et al., 2013). The OM/OC

ratios were 2.1 – 2.4 in the FT and 2.2 – 2.5 in the BL, with the same median of 2.3. In general, higher $f44$ is strongly

290   associated with increasing O/C and OM/OC ratio. These very high values of $f44$, O/C and OM/OC ratios consistently reflect

the highly oxidized and low volatility nature of OA during CLARIFY.

3.1.3 Enhancement ratios of BC and OA

The modified combustion efficiency (MCE) was calculated to indicate the combustion conditions at source (Yokelson et al., 2009). Details of the method of calculating MCE are listed in Supplementary S1. The MCEs of FT smoke were generally around 0.97 during CLARIFY, as shown in Fig. 5. An MCE of 0.9 is commonly used to indicate BB smoke predominantly influenced by combustion during the flaming phase (MCE > 0.9) whereas, MCE < 0.9 represents the smouldering phase (Reid et al., 2005). By this definition, CLARIFY smoke plumes transported from the southern Africa are likely to be mostly controlled by flaming-phase combustion at source.

The enhancement ratios of BC and OA were calculated by dividing them by the excess mixing ratio of the combustion tracer, CO, after background values had been removed (Lefer et al., 1994). The detailed calculation method is listed in Supplementary S1. These ratios ($\mu g\ m^{-3}$ / ppmv) can indicate the emission conditions of fire at source when both BC and CO are conserved over the timescales of transport in the absence of wet removal. The emission of BC is usually high during flaming combustion, while smouldering combustion tends to emit smoke high in CO and organic mass (e.g. Christian et al., 2003). For example, BC/ΔCO values from 9 to 28 and OA/ΔCO values from 23 to 82 were observed for BB source in flaming combustion, from measurements in Senegal (West African) (Capes et al., 2008), California (shrub and grass) (May et al., 2014) and Wyoming (west American shrub) (Pratt et al., 2011). A range of (1.7 – 6.5) for BC/ΔCO and (100 – 120) for OA/ΔCO, were reported for BB source in smouldering combustion (Capes et al., 2008; Kondo et al., 2011; May et al., 2014).

The BC/ΔCO and OA/ΔCO ratios ($\mu g\ m^{-3}$ / ppmv) were calculated in FT and BL smoke plumes separately for each flight and are shown in Fig. 5. In the BB-polluted FT, the medians of BC/ΔCO ratios from each flight ranged from 10.8 to 14.2 in period 2 and were higher (12.8 – 16.7) in period 3, while OA/ΔCO values were comparable between the two periods (period 2: 53 – 83; period 3: 55 – 79). In the BB-polluted BL, the BC/ΔCO and OA/ΔCO ratios in period 1 (12.8 – 14; 77 – 98) were higher than in period 3 (7.4 – 10.6; 30 – 51). For CLARIFY, particles observed in the FT have not encountered cloud and hence may not have been subject to significant removal processes during transport from Africa across the southeast Atlantic and are likely to be long-lived. Previous studies have reported the transatlantic transport of BB pollutants from Africa to the Amazon Basin (Baars et al., 2011; Andreae et al., 2015; Holanda et al., 2019). It is likely that observed BC/ΔCO values in FT smoke are similar to values at source. However OA/ΔCO may be more complex due to aging of primary organics (POA) and secondary organic aerosol (SOA) formation after emission (Yokelson et al., 2009;Cubison et al., 2011;Vakkari et al., 2018). During CLARIFY, BC/ΔCO ratios in FT smoke were in the reported range of BB sources controlled by flaming combustion. The slight variations between flights may be due to differences in emission if there is no significant removal process. Compared with the FT, BC/ΔCO and OA/ΔCO ratios were generally lower in the BL, clearly seen in period 3, indicating that a fraction of particles may be removed by cloud activation or scavenging and subsequent precipitation after FT aerosols mix into the BL. However, the ratios were not considerably lower than those in the FT, suggesting that the removal processes were inefficient. During period 3, the difference between BL and FT BC/ΔCO varied

from 20 to 45%, suggesting different scavenging fractions. In the BL, both the differences due to emission and the extent of

325 aerosol removal may cause the variation in the ratios.

3.2 Aerosol size distribution

We determined dry number size distributions from both PCASP and SMPS, during SLRs in the FT and BL separately. The mean size distributions of observed BBA from SLRs for each period are shown in Fig. 6a. During CLARIFY, we mainly detected a single dominant accumulation mode for both FT and BL BBA. The lognormal fitted count median

330 diameters (CMD) of mean size distributions derived from the PCASP were 232 nm and 202 nm for the BB-polluted FT and BL respectively. Fig. 6b shows the mean number size distribution for SLRs in the clean BL air masses in period 2. This indicates that new particle formation was occurring in the background marine environment, with a CMD of ~30 nm in the Aitken mode, and a CMD of ~160 nm in the accumulation mode.

Recent ground-based measurements of southern African savannah and grassland fires found a CMD of 69 nm in fresh

335 smoke (age < 0.5 h), which grew to 123 nm in the next three hours (Vakkari et al., 2018). CLARIFY observed BBA are much larger than those reported for fresh African smoke, this may be due to substantial coagulation and condensation during transport. However, Haywood et al. (2003a) reported a CMD of ~240 nm for aged BBA (1–2 days) off the Namibian coast and ~200 nm for fresh BBA (~ 5h) during SAFARI-2000. There is size similarity between SAFARI aged BBA (1–2 days) and more aged BBA (>7 days) in this study, despite the different ages of aerosols. This consistency validates a priori size

340 distribution assumptions for the aerosol model recently used in SEVIRI satellite retrievals of aerosols (CMD = 238 nm) made by Peers et al. (2019).

Vertical profiles of lognormal fitted CMDs calculated from the PCASP data are shown in Fig. 6c. There is a slightly increasing trend of CMDs with altitude (by ~5%) in the BB-polluted FT, and no significant vertical variability in the BL. CMDs in the BL are generally smaller than that in the FT, consistent with lower BC/ΔCO and OA/ΔCO ratios in the BL than

345 in the FT presented in the previous section and likely a result of more efficient removal of larger particles.

3.3 Aerosol single scattering albedo

Vertical profiles of dry SSA derived from EXSCALABAR measurements are shown in Fig. 7. The median value of SSA was calculated for each 400 m altitude bin. In the BB-polluted FT, SSA increased with altitude, varying from 0.83 to 0.88 at 405 nm and from 0.80 to 0.86 at 658 nm. In the BB-polluted BL during period 3, SSA decreased significantly with

350 increasing altitude. Close to the surface, the SSA was 0.86 at 405 nm and 0.85 at 658 nm, decreasing to 0.82 at 405 nm and 0.80 at 658 nm at the top of the BL. The BL median SSA in period 1 showed a weak vertical change and was higher than that in period 3.

Fig. 8 shows the CLARIFY SSA average values, compared with previous observation studies of southern African BB at different ages and covering various relevant regions. In the source region, the average SSA of fresh BBA measured during

355 SAFARI-2000 was 0.86, 0.84, and 0.80 at 450, 550, and 700 nm (Haywood et al., 2003a, b), aged BBA (1–2 days) usually

had a higher SSA (Haywood et al., 2003a, b; Johnson et al, 2008). However, SSA of more aged BBA (> 4 days, mainly in the FT) during ORACLES-2016 were observed to be lower than the SAFARI aged BBA (1–2 days) (Pistone et al., 2019). The CLARIFY observations presented in this study were made further west than the ORACLES region and undergone additional days of aging (>7 days since emission). The average SSA of CLARIFY FT BBA was (0.85 ± 0.02) at 405 nm and

360 (0.82 ± 0.03) at 658 nm, falling within the lowest level of the above reported range. The average SSA of CLARIFY BL BBA were (0.86 ± 0.02) at 405 nm and (0.84 ± 0.03) at 658 nm, higher than that in the FT. Ground-based in-situ SSA measurements made on Ascension Island in 2017 (Zuidema et al., 2018) are expected to be comparable to CLARIFY BL aerosols, while they observed the lowest values among previous observations of the southern African BBA.

These previous observations employed different measurement methods from those employed during CLARIFY, and

365 used the Particle Soot Absorption Photometer (PSAP) and nephelometer. Limitations with filter-based measurements of aerosol light absorption cannot be ignored (Lack et al., 2008; Davies et al., 2019). Davies et al. (2019) found that the mean SSA of aged BBA derived from CRDS coupled with filter-based methods, applying different correction schemes, are 0.01 – 0.04 lower than that measured from EXSCALABAR PAS and CRDS, which could explain some of the difference.

Despite the systematic variability between different measurement methods, the datasets mentioned above imply some

370 important information of SSA with distance from the African BB source to the remote region. Abel et al. (2003) showed the increase of SSA in the first 5 h after emission during SAFARI-2000, which is likely due to the condensation of scattering material and the change in BC morphology from a chain agglomerate to a more spheroidal shape as the particle collapses as it becomes coated. Despite this initial increase, observations of SSA in regions where the aerosols are highly aged (>4 days since emission), like the ORACLES, CLARIFY and ground-based measurements on Ascension Island, are close to or lower

375 than those sampled closer to source (<2 days). These observations show that BBA remains strongly absorbing from near the coast of southern Africa to the far-field region around Ascension Island, suggesting that models with too little absorption for aged BBA will under-estimate the warming effect of BBA over the southeast Atlantic.

4 Discussion

4.1 Factors influencing vertical variability

380 #### 4.1.1 In the FT

CLARIFY OA was highly oxidized which is characteristic of aged, low-volatile organic aerosol. Aerosol properties will be relatively insensitive to further aging processes of OA. The main feature in the vertical variability of aerosol properties in the CLARIFY region is the nitrate aerosol which makes a greater fractional contribution to PM1 at higher altitudes.

385 Individual aerosol layers at different altitudes may have different source or transport history, as evidenced by the back-trajectory studies in Haywood et al. (2020, in prep), very probably leading to variation in the fractional chemical

composition. Another reasonable explanation exists for increasing nitrate mass fraction with altitude, which is driven by chemical thermodynamics across large temperature gradients. CLARIFY measurements show that the nitrate aerosol was largely inorganic and existed in the form of ammonium nitrate (NH_4NO_3) in the FT (see Supplementary S2), which is a semi-

390 volatile and hygroscopic inorganic salt. During some flights, individual layers were well-mixed, indicated by a constant potential temperature throughout their depth. In these layers, increasing mass concentrations of nitrate and ammonium with increasing altitude were observed, while other species were relatively invariant with altitude. An example is shown in Supplementary Fig. S3. If the aerosols are mostly in solid phase, lower temperatures at higher altitudes can shift the gas-particle partitioning system between ammonia and nitrate toward aerosol phase and increase the formation of NH_4NO_3. The

395 intrusion of BB smoke in the FT during periods 2 and 3 increased specific humidity compared with the cleaner FT in period 1 (see Fig. 9), since the FT smoke tend to coexist with enhanced water vapor as discussed in Adebiyi et al. (2015). With relatively constant specific humidity in BB smoke over the vertical profile, the RH was observed to increase at higher altitudes, consistent with colder temperatures aloft (see Fig. 9). With the increasing ambient RH, aerosols are likely to acquire water at higher altitude, becoming liquid particles and allowing NH_4NO_3 to dissolve in the aerosol phase. In

400 summary, there is a greater chance for nitrate to be present in the aerosol phase in the colder and higher RH atmosphere encountered towards the top of the aerosol layers.

With higher nitrate mass fraction at higher altitudes, BC constituted a smaller mass fraction while BC number fraction remained relatively constant in the FT (see Fig. 10). This indicates that the additional nitrate is likely to be mostly internally mixed with existing particles. However, since we only observed slight vertical change of CMDs of the bulk aerosols in the

405 FT, it is likely that this internal mixing did not significantly alter the overall dry aerosol size distributions. SSA is closely related to the particle size and chemical composition. The slightly increased particle size and the larger fraction of scattering material at higher levels would consistently contribute to the increasing SSA with altitude observed during CLARIFY.

In this study, the calculated SSA from the PAS and CRDS instruments are for dry aerosols. It is well known that the increase in RH can result in an increase in aerosol scattering, since particle size and refractive index vary with particle water

410 content (e.g. Zieger et al., 2013; Burgos et al., 2019). In the CLARIFY region, increasing RH with altitude in the FT is likely to result in an increase in aerosol size and scattering, when aerosol particles are most likely to acquire water near the top of the aerosol layers (3.8–5 km). Previous studies have reported that aerosol absorption can be also affected by humidification. However, it is noted that most of studies considering the effect of humidification on aerosol absorption are under high values of RH (RH > 85%) (e.g. Brem et al., 2012). The RH of observed smoke in the FT during CLARIFY was rarely over 80%. If

415 there is little effect of humidity on absorption, we would expect that the impact of humidification is likely to increase SSA at higher levels, indicating a substantially larger vertical variation in SSA in the FT.

4.1.2 In the BL

The entrainment of FT smoke is a recognized source for BL BBA over the southeast Atlantic (Gordon et al., 2018; Zuidema et al., 2018; Haslett et al., 2019b). There are two important factors that are likely to alter aerosol properties after FT

420   BBA mix into the BL. The first factor is marine emissions in the BL and cloud processing, and the second is removal processes as evidenced by lower BC/ΔCO and OA/ΔCO ratios in the BL than in the FT.

Dimethyl sulfide (DMS) from oceanic biogenic emission is an important source of sulfate precursor, SO_2, and sulfate aerosol (Perraud et al., 2015). The clean BL described in Sect. 3 suggests new particle formation and a marine sulfate background. Some of these marine sulfates would become internally mixed with BBA either by condensation of H_2SO_4 or by

425   cloud processing, thus driving nitrate to evaporate into the gas phase and causing the loss of nitrate aerosol in the BL. Taylor et al., (2020, in prep) did not observe thicker BC coatings in the BL than those in the low FT, while in this study the sulfate mass fraction in the BL was significantly enhanced, suggesting that some of the marine sulfates would be also externally mixed with BBA. Sea salt particles from sea spray can also provide submicron particles which exhibit an SSA close to 1. The mixing of more scattering material from marine emissions can result in a higher SSA in the BL than in the FT.

430   The removal events usually occur via aerosol activation to form cloud droplets during in-cloud processing and subsequent removal of those droplets by precipitation, which would also facilitate below-cloud aerosol scavenging (Moteki et al., 2012; Taylor et al., 2014). In this study, OA dominated the aerosol composition and was characterised by high f44 which is closely associated with carboxylic acid content (Duplissy et al., 2011). The aerosols with a large proportion of inorganic species and OA are likely to be hygroscopic. Larger aerosol particles which are hygroscopic were preferentially

435   activated and scavenged during removal events in the BL, thus the dry CMDs of remaining bulk aerosols in the BL were smaller than those in the FT. However, the removal rates were not as significant as previous studies of BBA removal affected by strong precipitation events which show a scavenging fraction of over 80% (Taylor et al., 2014). This suggests that the scavenging efficiency of removal by drizzle in the BL was not large in the CLARIFY region. Our measurements show that the extent of this removal process is sufficient to reduce the dry CMD by ~10% (figure 6).

440   The BC mass and number fractions in the BL were both lower when close to the surface (see Fig. 10). This may suggest variations in the extent of external mixing between BBA and marine particles throughout the BL. In the CLARIFY region, the widespread stratocumulus clouds commonly lead to a decoupled BL (Lock et al., 2000; Gordon et al., 2018). Abel et al. (2019) showed an example structure of decoupled BL during period 3, with an unstable layer from the sea surface up to an altitude of about 600 to 700 m, and then another layer up to the main BL inversion. The surface layer is likely to have a

445   significant source of marine sulfates from secondary formation as well as submicron sea salt aerosol from sea spay. This could explain the higher sulfate mass fraction and higher SSA close to the sea surface.

These properties (chemical, size and optical) and variations that we have reported are all for dry aerosols in the BL. The RH in the BB-polluted BL was mostly over 80 % and up to 95 % at the BL top (Figure 9), which would result in significant aerosol growth and scattering enhancement. Based on a scattering enhancement factor of ~1.4 at RH of 80 % reported for

450   ORACLES (Pistone et al., 2019) and SAFARI (Magi et al., 2003) aged BBA, there will an increase of SSA by 0.03 – 0.05 in the BL, without considering absorption change. However, in reality, this value will be lower since absorption enhancement is suggested to be significant at high humidity (RH > 85%) (e.g. Brem et al., 2012), which likely have the opposite effect of

lowering SSA. Due to high uncertainties surrounding these competing effects, more quantification studies of humidification impacts on aerosol optical properties, are needed to detailly determine BL biomass burning SSA in this region.

4.2 Drivers of the low SSA

Previous measurements of fresh or transported BBA from forest fires in the Amazon, Siberia and North America reported a range of (2 – 9%) for the average BC mass fractions of BBA (Kondo et al., 2011; Sahu et al., 2012; Artaxo et al., 2013; Allan et al., 2014; Morgan et al., 2019). Corresponding average dry SSA (at ~550 nm) ranged from 0.88 to 0.97, using in-situ measurements with PSAP and nephelometer (Corr et al., 2012; Johnson et al., 2016; Laing et al., 2016). Compared with other BB-type regions, BBA during CLARIFY was richer in BC, with larger BC mass fraction and lower SSA. Many factors contribute to the larger BC mass fraction. Burning sources of the CLARIFY transported BB smoke were controlled by flaming combustion with very high MCE, indicating that the emission of BC is likely to be proportionally high. The burning fuel of southern Africa savanna is also suggested to have higher BC emission factors than forests or peat (Andreae et al., 2019). Both high MCE and the fuel type would lead to BC-rich smoke plumes at sources. OA loss induced by the aging process and volatilization of semi-volatile material during dilution are likely to further enhance the BC mass fraction. This is consistent with the chemical composition comparison between BBA of different ages from other relevant studies, detailed in Table 1. In the absence of significant removal over the south Atlantic, these BC-rich smoke plumes from the southern Africa fires lead to the high BC contents far offshore, even after >7 days transport. The high BC fraction leads to a large fraction of absorbing material in the sampled BBA and therefore contributes to the low observed SSA during CLARIFY.

The mass absorption cross-section (MAC = B_{Abs}/BC mass concentration) describes the absorption efficiency of BC particles. In the CLARIFY region, MAC was found to be much higher than the MAC of fresh, uncoated BC (MAC = 7.5 m^2 g^{-1} at 550 nm) suggested by Bond and Bergstrom (2006). Average MAC values from ground-based measurements at Ascension Island were reported as 15.1, 13.3 and 10.7 m^2 g^{-1} at 464, 529 and 648 nm respectively (Zuidema et al., 2018), higher MAC values (21.0, 15.1 and 12.2 m^2 g^{-1} at 405, 514 and 658 nm respectively) were observed from aircraft observations during CLARIFY (Taylor et al., 2020, in prep). The enhanced absorption could be due to the observed thick coatings on BC (Taylor et al., 2020, in prep), causing a lensing effect and additional absorption of sunlight (Lack et al., 2009). This would also contribute to the relatively low observed SSA.

The relatively low dry SSA measured during CLARIFY, as determined by highly sensitive and accurate measurements that are not subject to the artefacts of filter-based methods, is an important result. The SSA of aged BBA used in climate models is generally higher than the SSA in this study (e.g. Randles and Ramaswamy, 2010; Johnson et al., 2016). Further, the vertical profile of SSA shows the lowest value at low FT layer around 2000 m altitude (median: 0.83 at 405 nm and 0.80 at 658 nm), the air is also relatively dry (~20%) in this layer, meaning that the measured dry SSA is analogous to ambient condition. This is particularly important since the lowest SSA is immediately above the stratiform cloud, enhancing the positive radiative feedback associated with the aerosol direct effect. These findings indicate that the modelled climate effects

485 of BBA in this region need reassessment in future studies and the variation in SSA values in different BB regions should be considered.

5 Conclusions

We have presented a detailed study of BBA chemical, physical and optical properties from the CLARIFY aircraft campaign, based from Ascension Island in the southeast Atlantic Ocean. These are the first in-situ airborne measurements

490 providing aerosol vertical information in this area which is affected by long-range transport of southern African BBA every year and is important climatically. Our dataset complements previous observations of the southern African BBA and extends previous studies to a wider geographical range and to a greater age of smoke, and provides unique parameterizations with which to constrain global and regional climate models and predict radiative effects across this region.

BB smoke plumes during CLARIFY have been shown to be mostly controlled by flaming combustion at their sources

495 and BBA has not undergone significant removal processes before arrival in the CLARIFY region, since enhancement ratios of BC remain relatively high. Transported submicron BBA was mainly composed of OA ((50 – 60) % by mass) and BC ((8 – 15) % by mass), over the southeast Atlantic. The particles have undergone a significant aging process during >7 days transit from source, as indicated by highly oxidized and low-volatility OA and thickly coated BC (Taylor et al, 2020). CLARIFY data is a good representative of highly aged aerosols from the southern African BB.

500 The highly aged BBA in the CLARIFY region has relatively low SSA as they are rich in BC and the MAC of BC is high. We also observed the vertical variability of dry SSA, the lowest SSA (median: 0.83 at 405 nm and 0.80 at 658 nm) was generally in the low FT layer around 2000 m altitude. The measured BBA in the CLARIFY region is generally more absorbing than that is currently represented in many climate models. Considering these BBAs have a long lifetime and their spatial range spans thousands of kilometers, the modelled climate effects need re-assessment over this region.

505 In the CLARIFY region, observed vertical variations in SSA is likely to be a persistent feature, which is function of vertical variations in relative chemical composition, size and mixing state of these aerosols. In the FT, a main reason for vertical variability is the thermodynamic processing of inorganic nitrate driven by lower temperatures and higher RH at the top of the BBA layer. The increasing amount of condensed nitrates is likely to be internally mixed with existing particles, which alters the relative chemical composition but does not significantly change the aerosol size distributions. Increases in

510 the dry SSA with altitude are associated with larger fractions of scattering material and slightly increased particle size at higher levels. These effects describe the variation in the dry aerosol properties. However, considering the effect of elevated RH on aerosol scattering at higher altitudes, the vertical variation in SSA is likely to be more significant when adjusted to ambient conditions.

The aerosols in the BL are essentially separate from the FT. Once aerosols are entrained into the BL, the BBA

515 circulates independently of the aerosol above it owing to the strong inversion. There are two important factors affecting aerosol properties in the BL. One is marine emissions providing marine sulfate and sea salt, which can be internally or

externally mixed with BBA. Another one is the possible aerosol removal by drizzle, resulting in smaller bulk aerosol size distributions. A larger fraction of scattering material may lead to a higher average dry SSA in the BL than in the FT. Vertical variability of aerosol properties exists since the BL is commonly decoupled over the southeast Atlantic. A larger
520 concentration of marine sulfate or submicron sea salt is likely to be present in the surface layer than above, leading to more scattering material and therefore higher SSA.

These observations provide new information in a climatically important region and demonstrate that the persistence of strongly absorbing aerosol from southern African BB across wide regions of the south Atlantic is prevalent and must be taken into account when considering regional radiation interactions. The observed vertical variation in aerosol properties
525 throughout the BL and FT, especially SSA, should be also considered as part of any future studies which rely on prescribed aerosol composition and optical properties.

530

545

References

Abel, S. J., Haywood, J. M., Highwood, E. J., Li, J., and Buseck, P. R.: Evolution of biomass burning aerosol properties from an agricultural fire in southern Africa, Geophysical Research Letters, 30, 10.1029/2003gl017342, 2003.

550 Abel, S. J., Highwood, E. J., Haywood, J. M., and Stringer, M. A.: The direct radiative effect of biomass burning aerosols over southern Africa, Atmos. Chem. Phys., 5, 1999-2018, 10.5194/acp-5-1999-2005, 2005.

Abel, S. J., Barrett, P. A., Zuidema, P., Zhang, J., Christensen, M., Peers, F., Taylor, J. W., Crawford, I., Bower, K. N., and Flynn, M.: Open cells can decrease the mixing of free-tropospheric biomass burning aerosol into the south-east Atlantic boundary layer, Atmos. Chem. Phys. Discuss., https://doi.org/10.5194/acp-2019-738, in review, 2019.

555 Adachi, K., Moteki, N., Kondo, Y., and Igarashi, Y.: Mixing states of light-absorbing particles measured using a transmission electron microscope and a single-particle soot photometer in Tokyo, Japan, J. Geophys. Res. Atmos., 121, 9153–9164, doi:10.1002/2016JD025153, 2016.

Adebiyi, A. A., Zuidema, P., and Abel, S. J.: The Convolution of Dynamics and Moisture with the Presence of Shortwave Absorbing Aerosols over the Southeast Atlantic, Journal of Climate, 28, 1997-2024, 10.1175/jcli-d-14-00352.1, 2015.

560 Aiken, A. C., DeCarlo, P. F., Kroll, J. H., Worsnop, D. R., Huffman, J. A., Docherty, K. S., Ulbrich, I. M., Mohr, C., Kimmel, J. R., Sueper, D., Sun, Y., Zhang, Q., Trimborn, A., Northway, M., Ziemann, P. J., Canagaratna, M. R., Onasch, T. B., Alfarra, M. R., Prevot, A. S. H., Dommen, J., Duplissy, J., Metzger, A., Baltensperger, U., and Jimenez, J. L.: O/C and OM/OC Ratios of Primary, Secondary, and Ambient Organic Aerosols with High-Resolution Time-of-Flight Aerosol Mass Spectrometry, Environmental Science & Technology, 42, 4478-4485, 10.1021/es703009q, 2008.

565 Alfarra, M. R., Prevot, A. S., Szidat, S., Sandradewi, J., Weimer, S., Lanz, V. A., Schreiber, D., Mohr, M., and Baltensperger, U.: Identification of the mass spectral signature of organic aerosols from wood burning emissions, Environmental science & technology, 41, 5770-5777, 2007.

Allan, J. D., Morgan, W. T., Darbyshire, E., Flynn, M. J., Williams, P. I., Oram, D. E., Artaxo, P., Brito, J., Lee, J. D., and Coe, H.: Airborne observations of IEPOX-derived isoprene SOA in the Amazon during SAMBBA, Atmos. Chem. Phys., 14,
570 11393-11407, https://doi.org/10.5194/acp-14-11393-2014, 2014.

Andreae, M. O., and Merlet, P.: Emission of trace gases and aerosols from biomass burning, Global Biogeochemical Cycles, 15, 955-966, 10.1029/2000gb001382, 2001.

Andreae, M. O., Acevedo, O. C., Araùjo, A., Artaxo, P., Barbosa, C. G. G., Barbosa, H. M. J., Brito, J., Carbone, S., Chi, X., Cintra, B. B. L., da Silva, N. F., Dias, N. L., Dias-Júnior, C. Q., Ditas, F., Ditz, R., Godoi, A. F. L., Godoi, R. H. M.,
575 Heimann, M., Hoffmann, T., Kesselmeier, J., Könemann, T., Krüger, M. L., Lavric, J. V., Manzi, A. O., Lopes, A. P., Martins, D. L., Mikhailov, E. F., Moran-Zuloaga, D., Nelson, B. W., Nölscher, A. C., Santos Nogueira, D., Piedade, M. T. F., Pöhlker, C., Pöschl, U., Quesada, C. A., Rizzo, L. V., Ro, C.-U., Ruckteschler, N., Sá, L. D. A., de Oliveira Sá, M., Sales, C. B., dos Santos, R. M. N., Saturno, J., Schöngart, J., Sörgel, M., de Souza, C. M., de Souza, R. A. F., Su, H., Targhetta, N., Tóta, J., Trebs, I., Trumbore, S., van Eijck, A., Walter, D., Wang, Z., Weber, B., Williams, J., Winderlich, J., Wittmann, F.,

580   Wolff, S., and Yáñez-Serrano, A. M.: The Amazon Tall Tower Observatory (ATTO): overview of pilot measurements on ecosystem ecology, meteorology, trace gases, and aerosols, Atmos. Chem. Phys., 15, 10723–10776, https://doi.org/10.5194/acp-15-10723-2015, 2015.

Andreae, M. O.: Emission of trace gases and aerosols from biomass burning – an updated assessment, Atmos. Chem. Phys., 19, 8523–8546, https://doi.org/10.5194/acp-19-8523-2019, 2019.

585   Arangio, A. M., Slade, J. H., Berkemeier, T., Poschl, U., Knopf, D. A., and Shiraiwa, M.: Multiphase chemical kinetics of OH radical uptake by molecular organic markers of biomass burning aerosols: humidity and temperature dependence, surface reaction, and bulk diffusion, J Phys Chem A, 119, 4533-4544, 10.1021/jp510489z, 2015.

Artaxo, P., Rizzo, L. V., Brito, J. F., Barbosa, H. M., Arana, A., Sena, E. T., Cirino, G. G., Bastos, W., Martin, S. T., and Andreae, M. O.: Atmospheric aerosols in Amazonia and land use change: from natural biogenic to biomass burning

590   conditions, Faraday Discuss, 165, 203-235, 10.1039/c3fd00052d, 2013.

Baars, H., Ansmann, A., Althausen, D., Engelmann, R., Artaxo, P., Pauliquevis, T., and Souza, R.: Further evidence for significant smoke transport from Africa to Amazonia, Geophys. Res. Lett., 38, L20802, doi:10.1029/2011GL049200, 2011.

Bahreini, R., Ervens, B., Middlebrook, A. M., Warneke, C., de Gouw, J. A., DeCarlo, P. F., Jimenez, J. L., Brock, C. A., Neuman, J. A., 45 Ryerson, T. B., Stark, H., Atlas, E., Brioude, J., Fried, A., Holloway, J. S., Peischl, J., Richter, D.,

595   Walega, J., Weibring, P., Wollny, A. G., and Fehsenfeld, F. C.: Organic aerosol formation in urban and industrial plumes near Houston and Dallas, Texas, Journal of Geophysical Research, 114, D00F16, https://doi.org/10.1029/2008JD011493, 2009.

Bond, T. C. and Bergstrom, R. W.: Light absorption by carbonaceous particles: An investigative review, Aerosol Science and Technology, 40, 27–67, https://doi.org/10.1080/02786820500421521, 2006.

600   Brem, B. T., Mena Gonzalez, F. C., Meyers, S. R., Bond, T. C., and Rood, M. J.: Laboratory-Measured Optical Properties of Inorganic and Organic Aerosols at Relative Humidities up to 95%, Aerosol Science and Technology, 46, 178-190, 10.1080/02786826.2011.617794, 2012.

Burgos, M.A., Andrews, E., Titos, G., Alados-Arboledas, L., Baltensperger, U., Day, D., Jefferson, A., Kalivitis, N., Mihalpoulos, N., Sherman, J., Sun, J., Weingartner, E., Zieger, P.: A global view on the effect of water uptake on aerosol

605   particle light scattering. Sci Data 6, 157, doi:10.1038/s41597-019-0158-7, 2019

Capes, G., Johnson, B., McFiggans, G., Williams, P. I., Haywood, J., and Coe, H.: Aging of biomass burning aerosols over West Africa: Aircraft measurements of chemical composition, microphysical properties, and emission ratios, Journal of Geophysical Research, 113, 10.1029/2008jd009845, 2008.

Christian, T., Kleiss, B., Yokelson, R. J., Holzinger, R., Crutzen, P. J., Hao, W. M., Saharjo, B. H., and Ward, D. E.:

610   Comprehensive laboratory measurements of biomass-burning emissions: 1. Emissions from Indonesian, African, and other fuels, J. Geophys. Res., 108(D23), 4719, doi:10.1029/2003JD003704, 2003.

Corr, C. A., Hall, S. R., Ullmann, K., Anderson, B. E., Beyersdorf, A. J., Thornhill, K. L., Cubison, M. J., Jimenez, J. L., Wisthaler, A., and Dibb, J. E.: Spectral absorption of biomass burning aerosol determined from retrieved single scattering albedo during ARCTAS, Atmospheric Chemistry and Physics, 12, 10505-10518, 10.5194/acp-12-10505-2012, 2012.

615 Cotterell, M. I., Orr-Ewing, A. J., Szpek, K., Haywood, J. M., and Langridge, J. M.: The impact of bath gas composition on the calibration of photoacoustic spectrometers with ozone at discrete visible wavelengths spanning the Chappuis band, Atmos. Meas. Tech., 12, 2371–2385, https://doi.org/10.5194/amt-12-2371-2019, 2019.

Cubison, M. J., Ortega, A. M., Hayes, P. L., Farmer, D. K., Day, D., Lechner, M. J., Brune, W. H., Apel, E., Diskin, G. S., Fisher, J. A., Fuelberg, H. E., Hecobian, A., Knapp, D. J., Mikoviny, T., Riemer, D., Sachse, G. W., Sessions, W., Weber, R.

620 J., Weinheimer, A. J., Wisthaler, A., and Jimenez, J. L.: Effects of aging on organic aerosol from open biomass burning smoke in aircraft and laboratory studies, Atmospheric Chemistry and Physics, 11, 12049-12064, 10.5194/acp-11-12049-2011, 2011.

Das, S., Harshvardhan, H., Bian, H., Chin, M., Curci, G., Protonotariou, A. P., Mielonen, T., Zhang, K., Wang, H., and Liu, X.: Biomass burning aerosol transport and vertical distribution over the South African-Atlantic region, Journal of

625 Geophysical Research: Atmospheres, 122, 6391-6415, 10.1002/2016jd026421, 2017.

Davies, N. W., Cotterell, M. I., Fox, C., Szpek, K., Haywood, J. M., and Langridge, J. M.: On the accuracy of aerosol photoacoustic spectrometer calibrations using absorption by ozone, Atmospheric Measurement Techniques, 11, 2313-2324, 10.5194/amt-11-2313-2018, 2018.

Davies, N. W., Fox, C., Szpek, K., Cotterell, M. I., Taylor, J. W., Allan, J. D., Williams, P. I., Trembath, J., Haywood, J. M.,

630 and Langridge, J. M.: Evaluating biases in filter-based aerosol absorption measurements using photoacoustic spectroscopy, Atmos. Meas. Tech., 12, 3417–3434, https://doi.org/10.5194/amt12-3417-2019, 2019.

Drewnick, F., Hings, S. S., DeCarlo, P., Jayne, J. T., Gonin, M., Fuhrer, K., Weimer, S., Jimenez, J. L., Demerjian, K. L., Borrmann, S., and Worsnop, D. R.: A New Time-of-Flight Aerosol Mass Spectrometer (TOF-AMS)—Instrument Description and First Field Deployment, Aerosol Science and Technology, 39, 637-658, 10.1080/02786820500182040,

635 2005.

Duplissy, J., DeCarlo, P. F., Dommen, J., Alfarra, M. R., Metzger, A., Barmpadimos, I., Prevot, A. S. H., Weingartner, E., Tritscher, T., Gysel, M., Aiken, A. C., Jimenez, J. L., Canagaratna, M. R., Worsnop, D. R., Collins, D. R., Tomlinson, J., and Baltensperger, U.: Relating hygroscopicity and composition of organic aerosol particulate matter, Atmos. Chem. Phys., 11, 1155-1165, 10.5194/acp-11-1155-2011, 2011.

640 Edwards, D. P., Emmons, L. K., Gille, J. C., Chu, A., Attié, J. L., Giglio, L., Wood, S. W., Haywood, J., Deeter, M. N., Massie, S. T., Ziskin, D. C., and Drummond, J. R.: Satellite-observed pollution from Southern Hemisphere biomass burning, Journal of Geophysical Research, 111, 10.1029/2005jd006655, 2006.

Formenti, P., Elbert, W., Maenhaut, W., Haywood, J., Osborne, S., and Andreae, M. O.: Inorganic and carbonaceous aerosols during the Southern African Regional Science Initiative (SAFARI 2000) experiment: Chemical characteristics,

645 physical properties, and emission data for smoke from African biomass burning, Journal of Geophysical Research:
Atmospheres, 108, n/a-n/a, 10.1029/2002jd002408, 2003.

Formenti, P., D'Anna, B., Flamant, C., Mallet, M. D., Piketh, S. J., Schepanski, K., Waquet, F., Auriol, F., Brogniez, G.,
Burnet, F., Chaboureau, J.-P., Chauvigné, A., Chazette, P., Denjean, C., Desboeufs, K., Doussin, J.-F., Elguindi, N.,
Feuerstein, S., Gaetani, M., Giorio, C., Klopper, D., Mallet, M. D., Nabat, P., Monod, A., Solmon, F., Namwoonde, A.,
650 Chikwililwa, C., Mushi, R., Welton, E. J., Holben, B., Formenti, P., D'Anna, B., Flamant, C., Mallet, M. D., Piketh, S. J.,
Schepanski, K., Waquet, F., Auriol, F., Brogniez, G., Burnet, F., Chaboureau, J.-P., Chauvigné, A., Chazette, P., Denjean,
C., Desboeufs, K., Doussin, J.-F., Elguindi, N., Feuerstein, S., Gaetani, M., Giorio, C., Klopper, D., Mallet, M. D., Nabat, P.,
Monod, A., Solmon, F., Namwoonde, A., Chikwililwa, C., Mushi, R., Welton, E. J. and Holben, B.: The Aerosols, Radiation
and Clouds in southern Africa (AEROCLOsA) field campaign in Namibia: overview, illustrative observations and way
655 forward, B. Am. Meteor. Soc., 100, 1277–1298, https://doi.org/10.1175/BAMS-D-17-0278.1, 2019.

Fuzzi, S., Baltensperger, U., Carslaw, K., Decesari, S., Denier van der Gon, H., Facchini, M. C., Fowler, D., Koren, I.,
Langford, B., Lohmann, U., Nemitz, E., Pandis, S., Riipinen, I., Rudich, Y., Schaap, M., Slowik, J. G., Spracklen, D. V.,
Vignati, E., Wild, M., Williams, M., and Gilardoni, S.: Particulate matter, air quality and climate: lessons learned and future
needs, Atmospheric Chemistry and Physics, 15, 8217-8299, 10.5194/acp-15-8217-2015, 2015.

660 Gerbig, C., Schmitgen, S., Kley, D., Volz-Thomas, A., Dewey, K., and Haaks, D.: An improved fast-response vacuum-UV
resonance fluorescence CO instrument, J. Geophys. Res.-Atmos., 104, 1699–1704, https://doi.org/10.1029/1998JD100031,
1999.

Gordon, H., Field, P. R., Abel, S. J., Dalvi, M., Grosvenor, D. P., Hill, A. A., Johnson, B. T., Miltenberger, A. K., Yoshioka,
M., and Carslaw, K. S.: Large simulated radiative effects of smoke in the south-east Atlantic, Atmospheric Chemistry and
665 Physics, 18, 15261-15289, 10.5194/acp-18-15261-2018, 2018.

Haslett, S. L., Taylor, J. W., Deetz, K., Vogel, B., Babić, K., Kalthoff, N., Wieser, A., Dione, C., Lohou, F., Brito, J., Dupuy,
R., Schwarzenboeck, A., Zieger, P., and Coe, H.: The radiative impact of out-of-cloud aerosol hygroscopic growth during
the summer monsoon in southern West Africa, Atmos. Chem. Phys., 19, 1505–1520, https://doi.org/10.5194/acp-19-1505-
2019, 2019a.

670 Haslett, S. L., Taylor, J. W., Evans, M., Morris, E., Vogel, B., Dajuma, A., Brito, J., Batenburg, A. M., Borrmann, S.,
Schneider, J., Schulz, C., Denjean, C., Bourrianne, T., Knippertz, P., Dupuy, R., Schwarzenböck, A., Sauer, D., Flamant, C.,
Dorsey, J., Crawford, I., and Coe, H.: Remote biomass burning dominates southern West African air pollution during the
monsoon, Atmospheric Chemistry and Physics Discussions, 1-23, 10.5194/acp-2019-38, 2019b.

Haywood, J. M., S. R. Osborne, P. N. Francis, A. Keil, P. Formenti, M. O.Andreae, and P. H. Kaye, The mean physical and
675 optical properties ofbiomass burning aerosol measured by the C-130 aircraft during SAFARI2000,J. Geophys. Res.,108,
doi:10.1029/2002JD002226, in press,2003a.

21

Haywood, J. M., P. N. Francis, M. D. Glew, O. Dubovik, and B. Holben, Comparison of aerosol size distributions, radiative properties and opticaldepths determined by aircraft observations and sunphotometers duringSAFARI 2000, J. Geophys. Res.,108, doi:10.1029/2002JD002250, inpress, 2003b

680   Haywood, J. M., Abel, J. S., Barrett, P., Bellouin, N., Blyth, A., Bower, K. N., Brooks, M., Carslaw, K., Coe, H., Cotterell, M., Crawford, I., Davies, N., Dingley, E., Field, P., Formenti, P., Gordon, H., de Graaf, M., Herbert, R., Johnson, B., Jones, A. C., Langridge, J., Malavelle, F., Partridge, D. G., Peers, F., Redemann, J., Stier, P., Szpek, K., Taylor, J., Watson-Parris, D., Wood, R., Wu, H. H. and Zuidema, P., Overview of the CLoud-Aerosol-Radiation Interaction and Forcing: Year-2017 (CLARIFY-2017) measurement campaign, Atmos. Chem. Phys. Prep.

685   Holanda, B. A., Pöhlker, M. L., Saturno, J., Sörgel, M., Ditas, J., Ditas, F., Wang, Q., Donth, T., Artaxo, P., Barbosa, H. M. J., Braga, R., Brito, J., Cheng, Y., Dollner, M., Franco, M. A., Kaiser, J., Klimach, T., Knote, C., Krüger, O. O., Fütterer, D., Lavrič, J. V., Ma, N., Machado, L. A. T., Ming, J., Morais, F., Paulsen, H., Sauer, D., Schlager, H., Su, H., Weinzierl, B., Walser, A., Walter, D., Wendisch, M., Ziereis, H., Zöger, M., Pöschl, U., Andreae, M. O., and Pöhlker, C.: Influx of African biomass burning aerosol during the Amazonian dry season through layered transatlantic transport of black carbon-rich

690   smoke, Atmos. Chem. Phys. Discuss., https://doi.org/10.5194/acp-2019-775, in review, 2019.

Johnson, B. T., Osborne, S. R., Haywood, J. M., and Harrison, M. A. J.: Aircraft measurements of biomass burning aerosol over West Africa during DABEX, J. Geophys. Res., 113, D00C06, doi:10.1029/2007JD009451, 2008.

Johnson, B. T., Haywood, J. M., Langridge, J. M., Darbyshire, E., Morgan, W. T., Szpek, K., Brooke, J. K., Marenco, F., Coe, H., Artaxo, P., Longo, K. M., Mulcahy, J. P., Mann, G. W., Dalvi, M., and Bellouin, N.: Evaluation of biomass burning

695   aerosols in the HadGEM3 climate model with observations from the SAMBBA field campaign, Atmos. Chem. Phys., 16, 14657–14685, https://doi.org/10.5194/acp-16-14657-2016, 2016.

Jolleys, M. D., Coe, H., McFiggans, G., Taylor, J. W., O'Shea, S. J., Le Breton, M., Bauguitte, S. J.-B., Moller, S., Di Carlo, P., Aruffo, E., Palmer, P. I., Lee, J. D., Percival, C. J., and Gallagher, M. W.: Properties and evolution of biomass burning organic aerosol from Canadian boreal forest fires, Atmos. Chem. Phys., 15, 3077–3095, https://doi.org/10.5194/acp-15-

700   3077-2015, 2015.

Koch, D., and Del Genio, A. D.: Black carbon semi-direct effects on cloud cover: review and synthesis, Atmospheric Chemistry and Physics, 10, 7685-7696, 10.5194/acp-10-7685-2010, 2010.

Kondo, Y., Matsui, H., Moteki, N., Sahu, L., Takegawa, N., Kajino, M., Zhao, Y., Cubison, M. J., Jimenez, J. L., Vay, S., Diskin, G. S., Anderson, B., Wisthaler, A., Mikoviny, T., Fuelberg, H. E., Blake, D. R., Huey, G., Weinheimer, A. J., Knapp,

705   D. J., and Brune, W. H.: Emissions of black carbon, organic, and inorganic aerosols from biomass burning in North America and Asia in 2008, Journal of Geophysical Research, 116, 10.1029/2010jd015152, 2011.

Kuwata, M., Shao, W., Lebouteiller, R., and Martin, S. T.: Classifying organic materials by oxygen-to-carbon elemental ratio to predict the activation regime of Cloud Condensation Nuclei (CCN), Atmospheric Chemistry and Physics, 13, 5309-5324, 10.5194/acp-13-5309-2013, 2013.

710   Labonne, M., Bréon, F.-M., and Chevallier, F.: Injection height of biomass burning aerosols as seen from a spaceborne lidar, Geophysical Research Letters, 34, 10.1029/2007gl029311, 2007.

Laborde, M., Mertes, P., Zieger, P., Dommen, J., Baltensperger, U., and Gysel, M.: Sensitivity of the Single Particle Soot Photometer to different black carbon types, Atmos. Meas. Tech., 5, 1031– 1043, doi:10.5194/amt-5-1031-2012, 2012a.

Laborde, M., Schnaiter, M., Linke, C., Saathoff, H., Naumann, K.- H., Möhler, O., Berlenz, S., Wagner, U., Taylor, J. W.,
715   Liu, D., Flynn, M., Allan, J. D., Coe, H., Heimerl, K., Dahlkötter, F., Weinzierl, B., Wollny, A. G., Zanatta, M., Cozic, J., Laj, P., Hitzenberger, R., Schwarz, J. P., and Gysel, M.: Single Particle Soot Photometer intercomparison at the AIDA chamber, Atmos. Meas. Tech., 5, 3077–3097, doi:10.5194/amt-5-3077-2012, 2012b.

Lack, D. A., Cappa, C. D., Covert, D. S., Baynard, T., Massoli, P., Sierau, B., Bates, T. S., Quinn, P. K., Lovejoy, E. R., and Ravishankara, A. R.: Bias in Filter-Based Aerosol Light Absorption Measurements Due to Organic Aerosol Loading:
720   Evidence from Ambient Measurements, Aerosol Science and Technology, 42, 1033-1041, 10.1080/02786820802389277, 2008.

Lack, D. A., Cappa, C. D., Cross, E. S., Massoli, P., Ahern, A. T., Davidovits, P., and Onasch, T. B.: Absorption Enhancement of Coated Absorbing Aerosols: Validation of the Photo-Acoustic Technique for Measuring the Enhancement, Aerosol Science and Technology, 43, 1006-1012, 10.1080/02786820903117932, 2009.

725   Laing, J. R., Jaffe, D. A., and Hee, J. R.: Physical and optical properties of aged biomass burning aerosol from wildfires in Siberia and the Western USA at the Mt. Bachelor Observatory, Atmos. Chem. Phys., 16, 15185–15197, https://doi.org/10.5194/acp-16-15185-2016, 2016.

Lance, S., Brock, C. A., Rogers, D., and Gordon, J. A.: Water droplet calibration of the Cloud Droplet Probe (CDP) and in-flight performance in liquid, ice and mixed-phase clouds during ARCPAC, Atmos. Meas. Tech., 3, 1683–1706,
730   https://doi.org/10.5194/amt-3-1683-2010, 2010.

Lefer, B. L., Talbot, R. W., Harriss, R. C., Bradshaw, J. D., Sandholm, S. T., Olson, J. O., Sachse, G. W., Collins, J., Shipham, M. A., Blake, D. R., Klemm, K. I., Klemm, O., Gorzelska, K., and Barrick, J.: Enhancement of acidic gases in biomass burning impacted air masses over Canada, J. Geophys. Res., 99, 1721–1737, 1994.

Liu, D., Flynn, M., Gysel, M., Targino, A., Crawford, I., Bower, K., Choularton, T., Juryányi, Z., Steinbacher, M., Hüglin, C.,
735   Curtius, J., Kampus, M., Petzold, A., Weingartner, E., Baltensperger, U., and Coe, H.: Single particle characterization of black carbon aerosols at a tropospheric alpine site in Switzerland, Atmospheric Chemistry and Physics, 10, 7389-7407, 10.5194/acp-10-7389-2010, 2010.

Lock, A. P., Brown, A. R., Bush, M. R., Martin, G. M., and Smith, R. N. B.: A New Boundary Layer Mixing Scheme. Part I: Scheme Description and Single-Column Model Tests, Monthly Weather Review, 128, 3187-3199, 10.1175/1520-
740   0493(2000)128<3187:ANBLMS>2.0.CO;2, 2000.

Magi, B. I. and Hobbs, P. V.: Effects of humidity on aerosols in southern Africa during the biomass burning season, J. Geophys. Res., 108, 8495, doi:10.1029/2002jd002144, 2003.

Atmospheric
Chemistry
and Physics
Discussions

May, A. A., McMeeking, G. R., Lee, T., Taylor, J. W., Craven, J. S., Burling, I., Sullivan, A. P., Akagi, S., Collett Jr., J. L., Flynn, M., Coe, H., Urbanski, S. P., Seinfeld, J. H., Yokelson, R. J., and Kreidenweis, S. M.: Aerosol emissions from

745   prescribed fires in the United States: a synthesis of laboratory and aircraft measurements, J. Geophys. Res.-Atmos., 119, 11826–11849, doi:10.1002/2014JD021848, 2014.

McComiskey, A., Schwartz, S. E., Schmid, B., Guan, H., Lewis, E. R., Ricchiazzi, P., and Ogren, J. A.: Direct aerosol forcing: Calculation from observables and sensitivities to inputs, Journal of Geophysical Research, 113, 10.1029/2007jd009170, 2008.

750   McMeeking, G. R., Hamburger, T., Liu, D., Flynn, M., Morgan, W. T., Northway, M., Highwood, E. J., Krejci, R., Allan, J. D., Minikin, A., and Coe, H.: Black carbon measurements in the boundary layer over western and northern Europe, Atmospheric Chemistry and Physics, 10, 9393-9414, 10.5194/acp-10-9393-2010, 2010.

Middlebrook, A. M., Bahreini, R., Jimenez, J. L. and Canagaratna, M. R.: Evaluation of composition-dependent collection efficiencies for the Aerodyne Aerosol Mass Spectrometer using field data, Aerosol Sci. Technol., 46, 258- 271, 2012.

755   Morgan, W. T., Allan, J. D., Bower, K. N., Capes, G., Crosier, J., Williams, P. I., and Coe, H.: Vertical distribution of sub-micron aerosol chemical composition from North-Western Europe and the North-East Atlantic, Atmos. Chem. Phys., 9, 5389-5401, 10.5194/acp-9-5389-2009, 2009.

Morgan, W. T., Allan, J. D., Bauguitte, S., Darbyshire, E., Flynn, M. J., Lee, J., Liu, D., Johnson, B., Haywood, J., Longo, K. M., Artaxo, P. E., and Coe, H.: Transformation and aging of biomass burning carbonaceous aerosol over tropical South

760   America from aircraft in-situ measurements during SAMBBA, Atmos. Chem. Phys. Discuss., https://doi.org/10.5194/acp-2019-157, in review, 2019.

Moteki, N., Kondo, Y., Oshima, N., Takegawa, N., Koike, M., Kita, K., Matsui, H., and Kajino, M.: Size dependence of wet removal of black carbon aerosols during transport from the boundary layer to the free troposphere, Geophys. Res. Lett., 39, L13802, doi:10.1029/2012GL052034, 2012.

765   Ng, N. L., Canagaratna, M. R., Jimenez, J. L., Chhabra, P. S., Seinfeld, J. H., and Worsnop, D. R.: Changes in organic aerosol composition with aging inferred from aerosol mass spectra, Atmospheric Chemistry and Physics, 11, 6465-6474, 10.5194/acp-11-6465-2011, 2011.

O'Shea, S. J., Bauguitte, S. J.-B., Gallagher, M. W., Lowry, D., and Percival, C. J.: Development of a cavity-enhanced absorption spectrometer for airborne measurements of CH_4 and CO_2, Atmos. Meas. Tech., 6, 1095–1109,

770   https://doi.org/10.5194/amt6-1095-2013, 2013.

Painemal, D., Kato, S., and Minnis, P.: Boundary layer regulation in the southeast Atlantic cloud microphysics during the biomass burning season as seen by the A-train satellite constellation, Journal of Geophysical Research: Atmospheres, 119, 11,288-211,302, 10.1002/2014jd022182, 2014.

Peers, F., Bellouin, N., Waquet, F., Ducos, F., Goloub, P., Mollard, J., Myhre, G., Skeie, R. B., Takemura, T., Tanré, D.,

775   Thieuleux, F., and Zhang, K.: Comparison of aerosol optical properties above clouds between POLDER and AeroCom

models over the South East Atlantic Ocean during the fire season, Geophysical Research Letters, 43, 3991-4000, 10.1002/2016gl068222, 2016.

Peers, F., Francis, P., Fox, C., Abel, S. J., Szpek, K., Cotterell, M. I., Davies, N. W., Langridge, J. M., Meyer, K. G., Platnick, S. E., and Haywood, J. M.: Observation of absorbing aerosols above clouds over the south-east Atlantic Ocean

780 from the geostationary satellite SEVIRI – Part 1: Method description and sensitivity, Atmos. Chem. Phys., 19, 9595–9611, https://doi.org/10.5194/acp-19-9595-2019, 2019.

Perraud, V., Horne, J. R., Martinez, A. S., Kalinowski, J., Meinardi, S., Dawson, M. L., Wingen, L. M., Dabdub, D., Blake, D. R., Gerber, R. B., and Finlayson-Pitts, B. J.: The future of airborne sulfur-containing particles in the absence of fossil fuel sulfur dioxide emissions, Proceedings of the National Academy of Sciences, 112, 13514-13519, 10.1073/pnas.1510743112,

785 2015.

Pistone, K., Redemann, J., Doherty, S., Zuidema, P., Burton, S., Cairns, B., Cochrane, S., Ferrare, R., Flynn, C., Freitag, S., Howell, S. G., Kacenelenbogen, M., LeBlanc, S., Liu, X., Schmidt, K. S., Sedlacek III, A. J., Segal-Rozenhaimer, M., Shinozuka, Y., Stamnes, S., van Diedenhoven, B., Van Harten, G., and Xu, F.: Intercomparison of biomass burning aerosol optical properties from in situ and remote-sensing instruments in ORACLES-2016, Atmos. Chem. Phys., 19, 9181–9208,

790 https://doi.org/10.5194/acp-19-9181-2019, 2019.

Pratt, K. A., Murphy, S. M., Subramanian, R., DeMott, P. J., Kok, G. L., Campos, T., Rogers, D. C., Prenni, A. J., Heymsfield, A. J., Seinfeld, J. H., and Prather, K. A.: Flight-based chemical characterization of biomass burning aerosols within two prescribed burn smoke plumes, Atmospheric Chemistry and Physics, 11, 12549-12565, 10.5194/acp-11-12549-2011, 2011.

795 Rajapakshe, C., Zhang, Z., Yorks, J. E., Yu, H., Tan, Q., Meyer, K., Platnick, S., and Winker, D. M.: Seasonally transported aerosol layers over southeast Atlantic are closer to underlying clouds than previously reported, Geophysical Research Letters, 44, 5818-5825, 10.1002/2017gl073559, 2017.

Randles, C. A. and Ramaswamy, V.: Direct and semi-direct impacts of absorbing biomass burning aerosol on the climate of southern Africa: a Geophysical Fluid Dynamics Laboratory GCM sensitivity study, Atmos. Chem. Phys., 10, 9819-9831,

800 https://doi.org/10.5194/acp-10-9819-2010, 2010.

Reid, J. S., Koppmann, R., Eck, T. F., and Eleuterio, D. P.: A review of biomass burning emissions part II: intensive physical properties of biomass burning particles, Atmos. Chem. Phys., 5, 799-825, 10.5194/acp-5-799-2005, 2005.

Rosenberg, P. D., Dean, A. R., Williams, P. I., Dorsey, J. R., Minikin, A., Pickering, M. A., and Petzold, A.: Particle sizing calibration with refractive index correction for light scattering optical particle counters and impacts upon PCASP and CDP

805 data collected during the Fennec campaign, Atmos. Meas. Tech., 5, 1147–1163, https://doi.org/10.5194/amt-5-1147-2012, 2012.

Sahu, L. K., Kondo, Y., Moteki, N., Takegawa, N., Zhao, Y., Cubison, M. J., Jimenez, J. L., Vay, S., Diskin, G. S., Wisthaler, A., Mikoviny, T., Huey, L. G., Weinheimer, A. J., and Knapp, D. J.: Emission characteristics of black carbon in

anthropogenic and biomass burning plumes over California during ARCTAS-CARB 2008, Journal of Geophysical Research:

810   Atmospheres, 117, n/a-n/a, 10.1029/2011jd017401, 2012.

Samset, B. H., Myhre, G., Schulz, M., Balkanski, Y., Bauer, S., Berntsen, T. K., Bian, H., Bellouin, N., Diehl, T., Easter, R. C., Ghan, S. J., Iversen, T., Kinne, S., Kirkevåg, A., Lamarque, J. F., Lin, G., Liu, X., Penner, J. E., Seland, Ø., Skeie, R. B., Stier, P., Takemura, T., Tsigaridis, K., and Zhang, K.: Black carbon vertical profiles strongly affect its radiative forcing uncertainty, Atmospheric Chemistry and Physics, 13, 2423-2434, 10.5194/acp-13-2423-2013, 2013.

815   Schneider, J., Weimer, S., Drewnick, F., Borrmann, S., Helas, G., Gwaze, P., Schmid, O., Andreae, M. O., and Kirchner, U.: Mass spectrometric analysis and aerodynamic properties of various types of combustion-related aerosol particles, International Journal of Mass Spectrometry, 258, 37-49, 10.1016/j.ijms.2006.07.008, 2006.

Seinfeld, J. and Pandis, S.: Atmospheric Chemistry and Physics: From Air Pollution to Climate Change, John Wiley and Sons, Inc., Hoboken, New Jersey, 2016.

820   Szpek, K., Cotterell, M.I., Davies, N.W., Fox, C., Tiddeman, D., Wilson, A., Bowles, J., King, R., Kent, J., Smout-Day, R., Richardson, M.S., Haywood, J.M., and Langridge, J.M. (2020). EXSCALABAR - a new instrument for high accuracy measurement of aerosol absorption and extinction from research aircraft. Atmos. Meas. Tech. Prep.

Tans, P., Zhao, C., and Kitzis, D.: The WMO Mole Fraction Scales for CO2 and other greenhouse gases, and uncertainty of the atmospheric measurements, in: 15th WMO/IAEA Meeting of Ex- perts on Carbon Dioxide, Other Greenhouse Gases,

825   and Related Tracer Measurement Techniques, Jena, Germany, 7–10 September

Taylor, J. W., Allan, J. D., Allen, G., Coe, H., Williams, P. I., Flynn, M. J., Le Breton, M., Muller, J. B. A., Percival, C. J., Oram, D., Forster, G., Lee, J. D., Rickard, A. R., Parrington, M., and Palmer, P. I.: Size-dependent wet removal of black carbon in Canadian biomass burning plumes, Atmos. Chem. Phys., 14, 13755-13771, https://doi.org/10.5194/acp-14-13755-2014, 2014.

830   Taylor, J. W., Allan, J. D., Liu, D., Flynn, M., Weber, R., Zhang, X., Lefer, B. L., Grossberg, N., Flynn, J., and Coe, H.: Assessment of the sensitivity of core / shell parameters derived using the single-particle soot photometer to density and refractive index, Atmospheric Measurement Techniques, 8, 1701-1718, 10.5194/amt-8-1701-2015, 2015.

Taylor, J. W., Wu, H. H., Szpek, K., Bower, K., Crawfield, I., Flynn, J. M., Williams, I. P., Dorsey, J., Langridge, J., Cotterell, M., Fox, C., Davies, N., Haywood, J. M., and Coe H., Absorption closure in aged biomass burning smoke using

835   different optical models, Atmos. Chem. Phys. Prep.

Trembath, J.: Airborne CCN Measurements, SAES, University of Manchester, UK, 2012.

Trembath, J., Bart, M., and Brooke, J.: FAAM Technical Note 01: Efficiencies of Modified Rosemount Housings for Sampling Aerosol on a Fast Atmospheric Research Aircraft, Tech. Rep. December, Facility for Airborne Atmospheric Measurement (FAAM), 2012.

840   Vakkari, V., Beukes, J. P., Dal Maso, M., Aurela, M., Josipovic, M., and van Zyl, P. G.: Major secondary aerosol formation in southern African open biomass burning plumes, Nature Geoscience, 10.1038/s41561-018-0170-0, 2018.

van der Werf, G. R., Randerson, J. T., Giglio, L., Collatz, G. J., Mu, M., Kasibhatla, P. S., Morton, D. C., DeFries, R. S., Jin,

Y., and van Leeuwen, T. T.: Global fire emissions and the contribution of deforestation, savanna, forest, agricultural, and peat fires (1997–2009), Atmospheric Chemistry and Physics, 10, 11707-11735, 10.5194/acp-10-11707-2010, 2010.

845   Voulgarakis, A., Marlier, M. E., Faluvegi, G., Shindell, D. T., Tsigaridis, K., and Mangeon, S.: Interannual variability of tropospheric trace gases and aerosols: The role of biomass burning emissions, Journal of Geophysical Research: Atmospheres, 120, 7157-7173, 10.1002/2014jd022926, 2015.

Yokelson, R. J., Crounse, J., DeCarlo, P., Karl, T., Urbanski, S., Atlas, E., Campos, T., Shinozuka, Y., Kasputin, V., Clarke, A., Weinheimer, A. J., Knapp, D., Montzka, D. D., Holloway, J., Weibring, P., Flocke, F., Zheng, W., Toohey, D., Wennberg,

850   P. O., Wiedinmyer, C., Mauldin, L., Fried, A., Richter, D., Walega, J., Jimenez, J. L., Adachi, K., Buseck, P. R., Hall, S. R., and Shetter, R.: Emissions from biomass burning in the Yucatan, Atmospheric Chemistry and Physics, 9, 5785, 2009.

Yokelson, R. J., Andreae, M. O., and Akagi, S. K.: Pitfalls with the use of enhancement ratios or normalized excess mixing ratios measured in plumes to characterize pollution sources and aging, Atmos. Meas. Tech., 6, 2155–2158, https://doi.org/10.5194/amt-6-2155-2013, 2013.

855   Zhang, Q., Jimenez, J. L., Worsnop, D. R., and Canagaratna, M.: A Case Study of Urban Particle Acidity and Its Influence on Secondary Organic Aerosol, Environmental Science & Technology, 41, 3213-3219, 10.1021/es061812j, 2007.

Zieger, P., Fierz-Schmidhauser, R., Weingartner, E., and Baltensperger, U.: Effects of relative humidity on aerosol light scattering: results from different European sites, Atmos. Chem. Phys., 13, 10609-10631, https://doi.org/10.5194/acp-13-10609-2013, 2013.

860   Zhou, J.: Hygroscopic Properties of Atmospheric Aerosol Particles in Various Environments, Doctoral dissertation, Lund University, Lund, ISBN:91-7874-120-3, 14–20, 2001.

Zuidema, P., Redemann, J., Haywood, J., Wood, R., Piketh, S., Hipondoka, M., and Formenti, P.: Smoke and Clouds above the Southeast Atlantic Upcoming Field Campaigns Probe Absorbing Aerosol's Impact on Climate, B. Am. Meteorol. Soc., 97, 1131– 1135, https://doi.org/10.1175/BAMS-D-15-00082.1, 2016.

865   Zuidema, P., Sedlacek, A. J., Flynn, C., Springston, S., Delgadillo, R., Zhang, J., Aiken, A. C., Koontz, A., and Muradyan, P.: The Ascension Island Boundary Layer in the Remote Southeast Atlantic is Often Smoky, Geophysical Research Letters, 45, 4456-4465, 10.1002/2017gl076926, 2018.
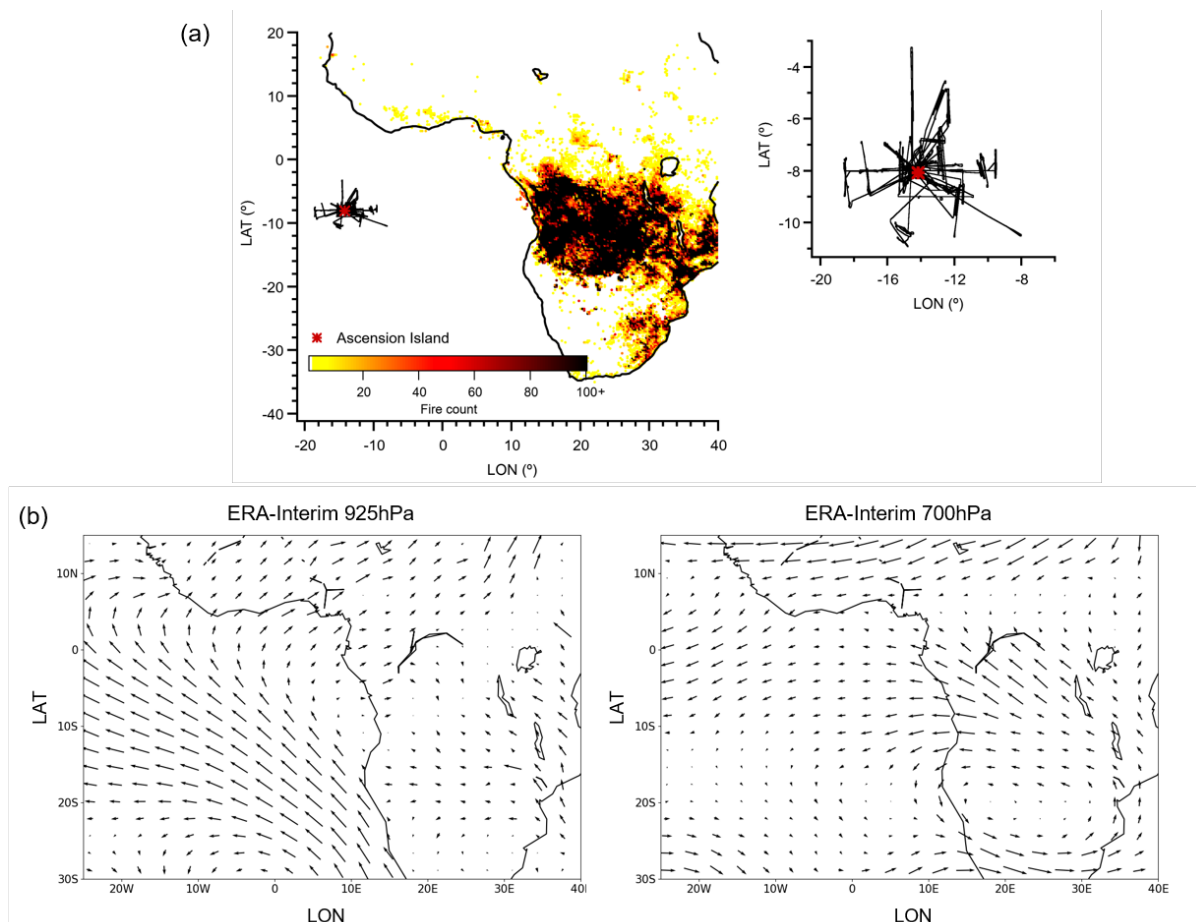
870 **Figure 1: (a) The integrated spatial distribution of MODIS-detected fire counts in August 2017, coupled with flight tracks (without transit flights) during CLARIFY-2017 aircraft campaign (16th August-7th September). (b) Average wind speed and direction at 925hPa (left) and 700hPa (right) in ERA-Interim re-analysis for August 2017. The length of arrow indicates wind speed.**
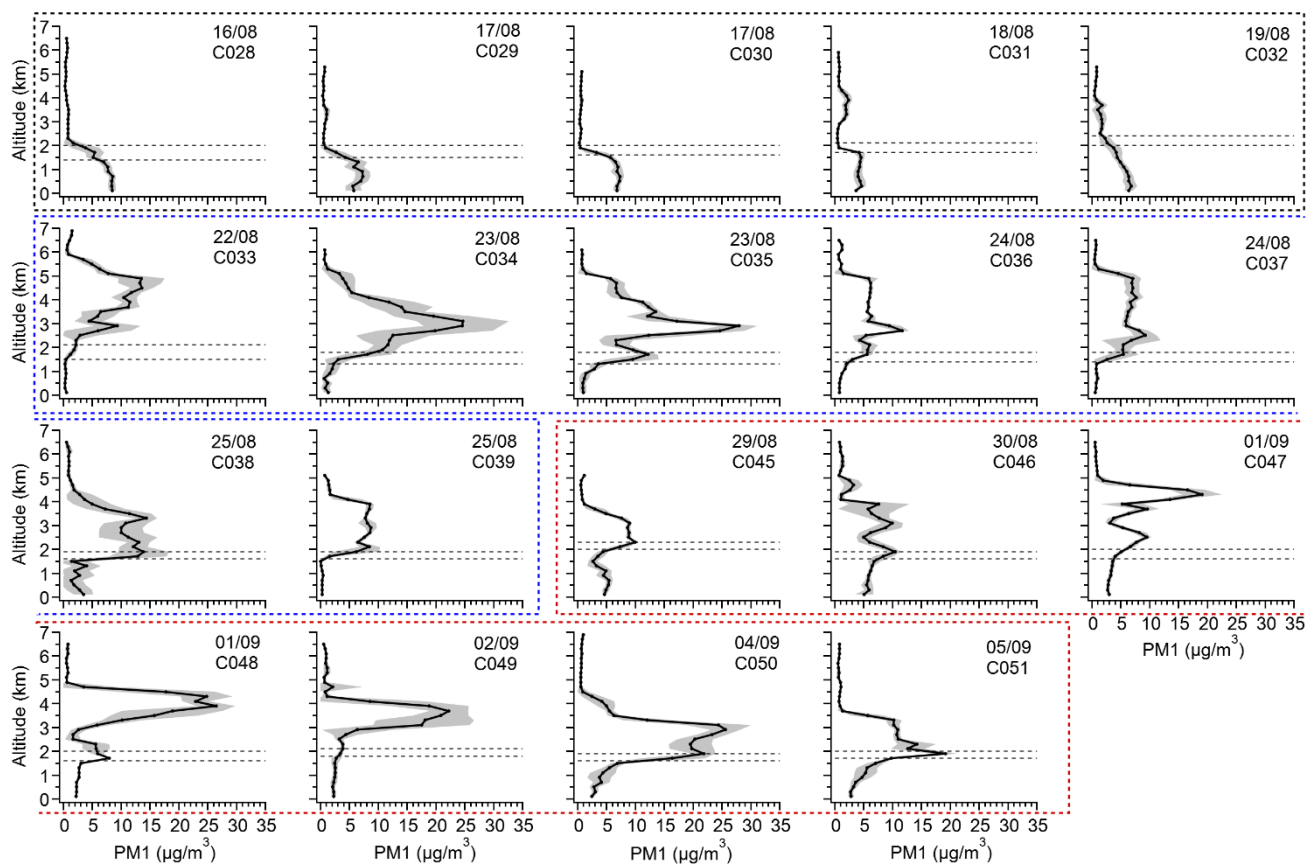
Figure 2: The average vertical distribution of submicron aerosol (PM1) in flights used in this study. PM1 is calculated from AMS non-refractory submicron species and SP2 BC. The grey shades represent standard deviation. The dashed lines represent the lower and upper level of the inversion layer. Period 1 is marked by black dashed square, period 2 is marked by blue, period 3 is marked by red.
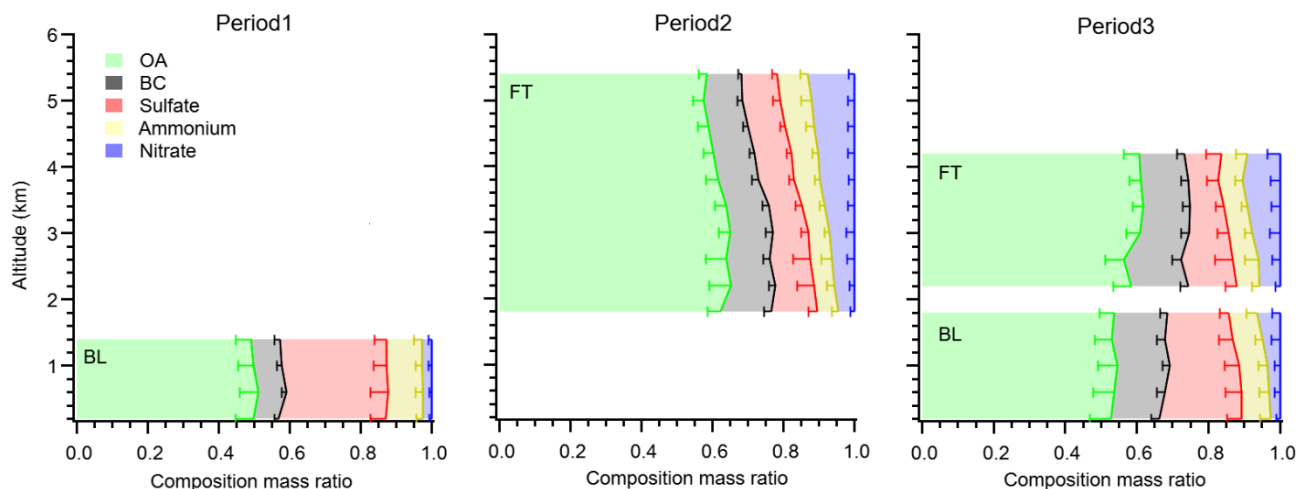
Figure 3: The average vertical distribution of PM1 chemical composition ratios in the BB-polluted FT and BL separately in each period. The width of color bars represents average mass ratio of different species in every 400 m bin. The error bars represent one standard deviation.

885
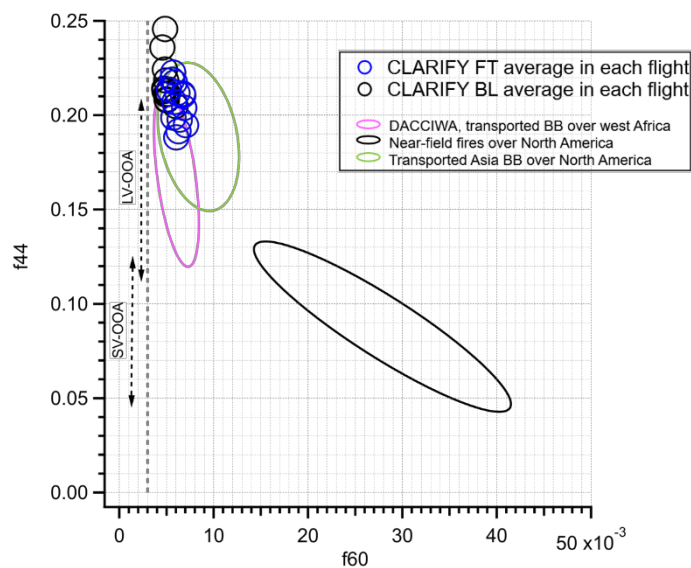
Figure 4: The fractional signals $f44$ vs $f60$ of aerosols sampled in this and other studies. Blue and black markers represent the average of FT and BL BBA layers, respectively, for each flight. The oval regions represent value ranges from other studies. The dashed grey line indicates the background of $f60$ (0.3%) under non-BB conditions, as
890 **recommended by Cubison et al. (2011).**
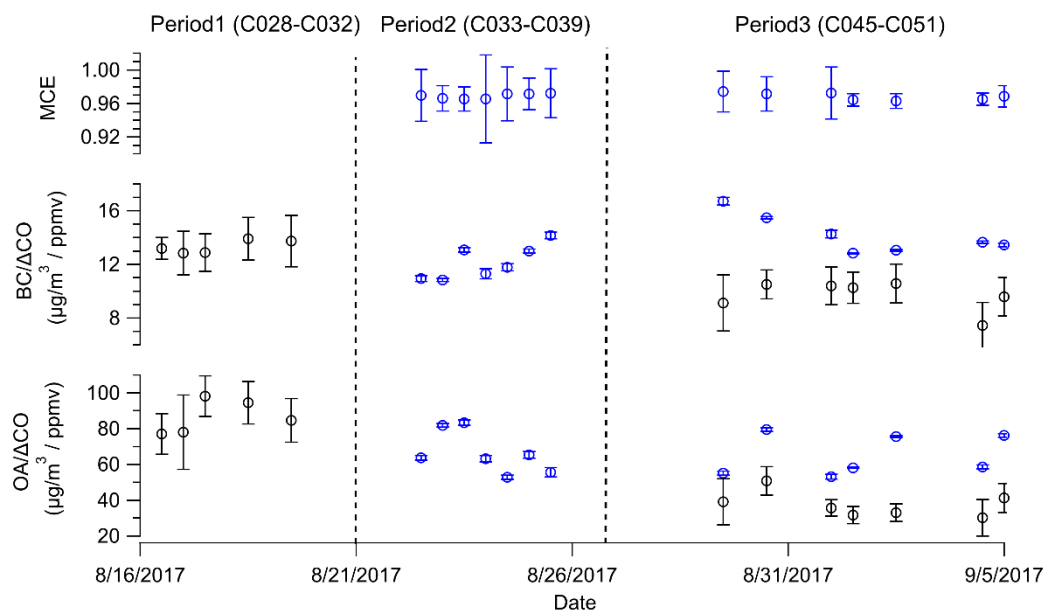
Figure 5: Top panel: the calculated MCE of CLARIFY FT plumes for each flight. The error bars show one standard deviation. Middle and bottom panels: the calculated BC/ΔCO and OA/ΔCO in FT and BL smoke plumes for each flight, the blue markers and error bars represent the fitted slopes and standard deviation from unconstrained linear orthogonal distance regression (ODR) in the FT, the black markers and errors represent the average and standard deviation of calculated ratios in the BL.
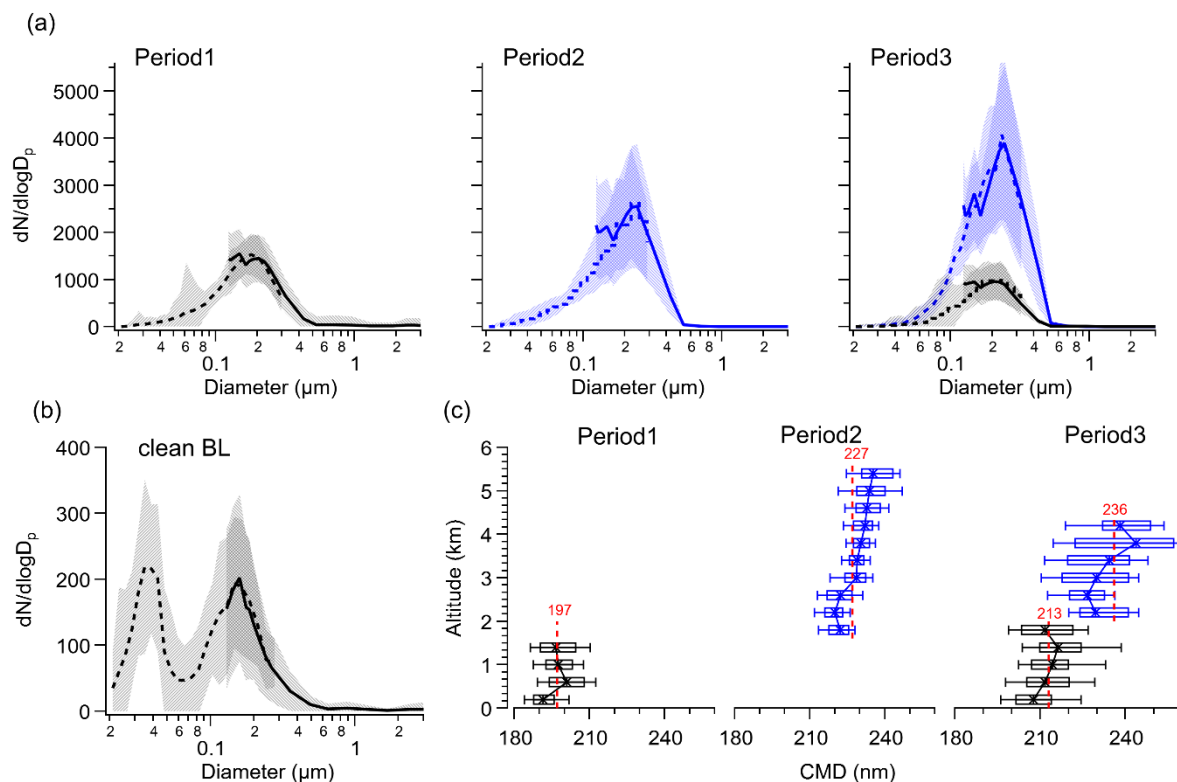
Figure 6: (a) The average size distributions of SLRs in the BB-polluted FT (blue) and BL (black) for each period. The solid lines represent results from PCASP, dashed lines represent results from SMPS. The blue lines and shading show mean and standard deviation from the FT, the black represent the BL. (b) The average size distribution of SLRs in the clean BL. (c) The vertical distribution of lognormal fitted count median diameters (CMD) from the PCASP. The boxes and whiskers indicate the 10%, 25%, median, 75% and 90% in every 400m bin in the BB-polluted FT (blue) and BL (black). The red dashed lines and numbers represent the lognormal fitted CMD of mean size distribution in the BB-polluted FT (blue) and BL (black) for each period.
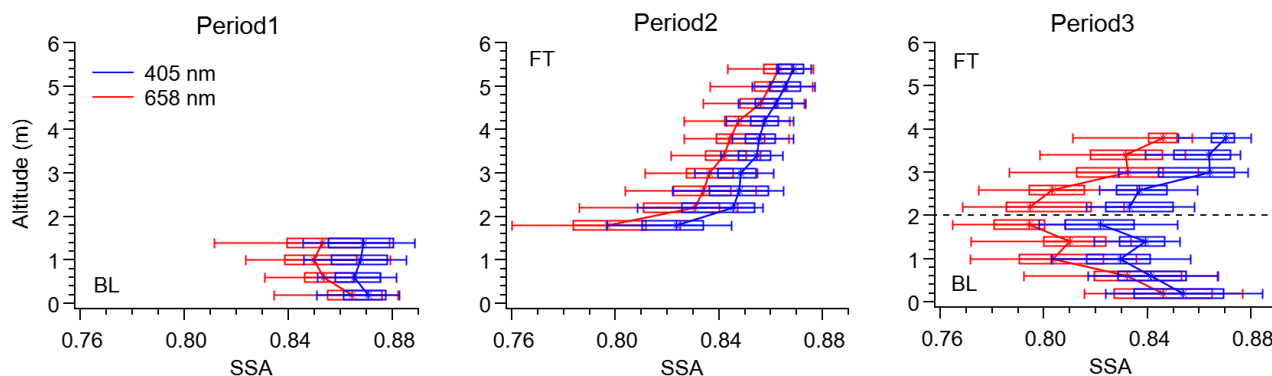
Figure 7: The vertical distribution of SSA at 405nm (blue) and 658nm (red) in BB-polluted FT and BL for each period. The boxes and whiskers represent 10%, 25%, median, 75% and 90% in every 400m bin.

915
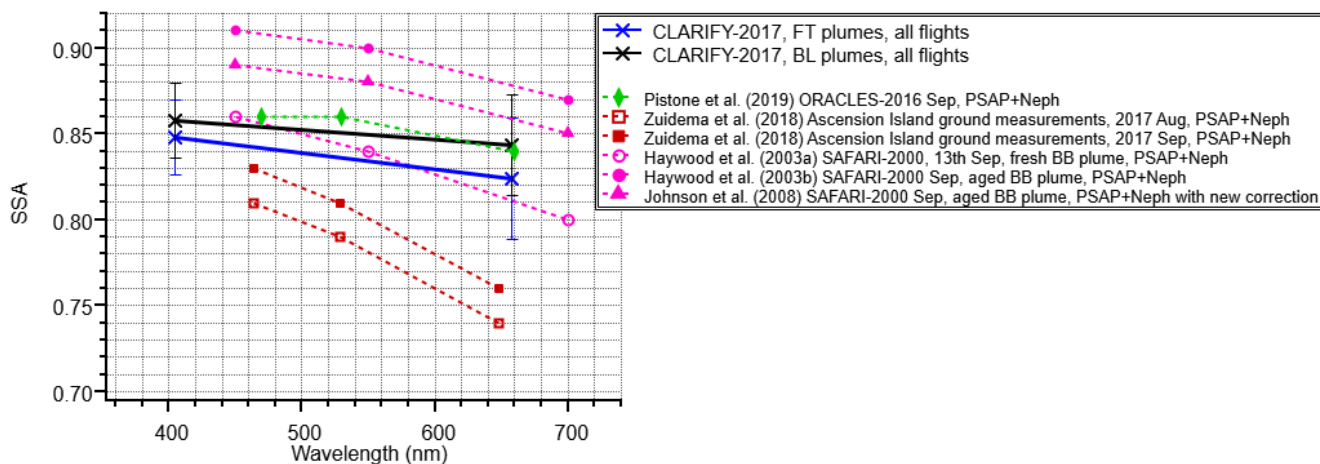
Figure 8: Wavelength dependence of the average SSA in FT and BL BBA for all flights used in this study. The
920 **markers and lines represent the mean value and standard deviation. The average SSA from previous studies in this region are shown for comparison.**

Atmospheric
Chemistry
and Physics
Discussions
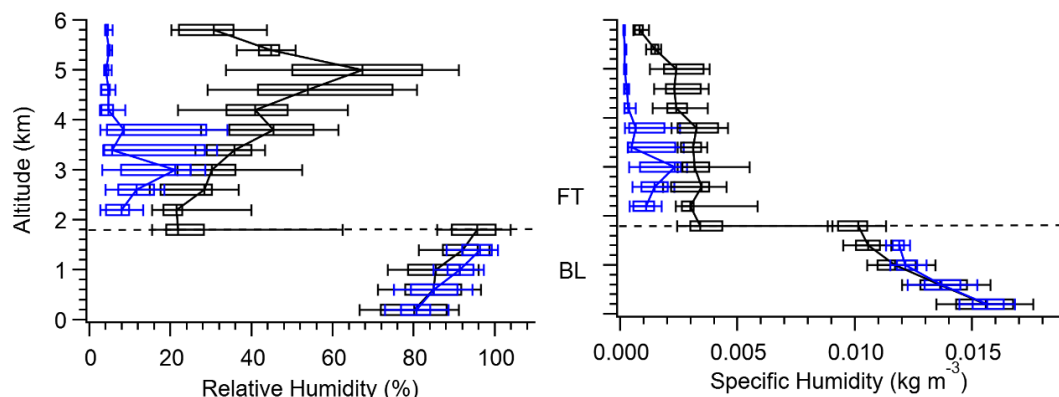
Figure 9: The vertical distribution of RH (left panel) and specific humidity (right panel) for clean (blue) and BB-polluted (black) conditions. Data for BB-polluted conditions are composited from periods 2 and 3 for FT BBA and periods 1 and 3 for BL BBA. Blue indicates the RH under clean conditions, sampled during period 1 in the FT and period 2 in the BL. The boxes and whiskers represent 10%, 25%, median, 75% and 90% in every 400m bin.
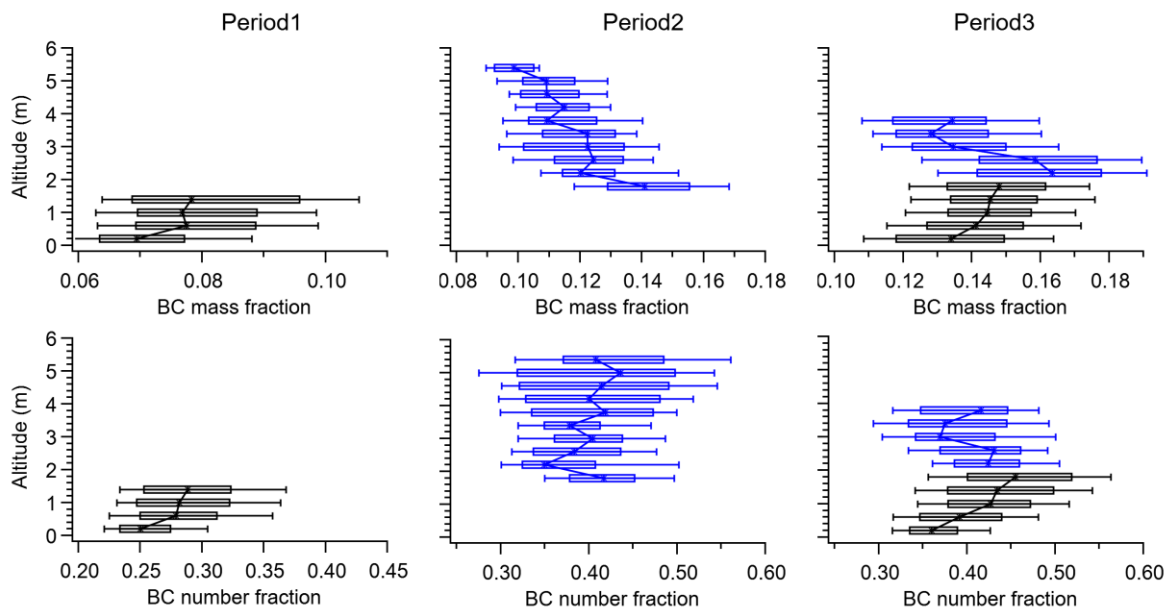
Figure 10: The vertical distribution of BC mass fraction and number fraction in BB-polluted FT (blue) and BL (black) for each period. The boxes and whiskers represent 10%, 25%, median, 75% and 90% in every 400m bin.

Table 1. The summary of CLARIFY aerosol composition and comparison with other studies of southern African BB

		Origination	OA mass fraction	BC mass fraction	Nitrate mass fraction	Ammonium mass fraction	Sulfate mass fraction	Reference
CLARIFY BB-polluted FT	Period 2	Transported	63 ± 5	13 ± 2	8 ± 3	7 ± 2	11 ± 3	This study
	Period 3	Transported	60 ± 5	15 ± 3	8 ± 3	7 ± 3	12 ± 4	This study
CLARIFY BB-polluted BL	Period 1	Transported	50 ± 5	8 ± 2	2 ± 1	10 ± 2	30 ± 4	This study
	Period 3	Transported	54 ± 6	14 ± 2	3 ± 2	8 ± 3	21 ± 5	This study
CLARIFY clean BL[1]	Period 2	Transported	~24	-	-	~16	~60	This study
SAFARI-2000, fresh plume		Near-source	85	5	3	3	4	Formenti et al., 2003[2]
SAFARI-2000, aged plume (1-2 days)		Near-source	71	6	6	5	12	Formenti et al., 2003[2]
DACCIWA West Africa, FT aged BB		Transported	~65	-	~10	~10	~15	Haslett et al., 2019b[3]
DACCIWA West Africa, Marine layer, aged BB		Transported	~58	-	~2	~10	~30	Haslett et al., 2019b[3]

Note: 1. The nitrate and BC concentrations were around zero, have large uncertainty and are therefore not provided here. 2. Formenti et al. (2003) used a factor of 2 to convert measured organic carbon (OC) to organic mass. It should be noted that BC was not measured optically for blackness as SP2 in this study, but instead for the elemental carbon (EC). 3. The fraction of BC is not provided by Haslett et al. (2019b), only data from AMS is calculated and hence the mass fractions of the non-BC components are likely elevated.